(A)

(B)

(C)

(D)

Figure 3. Stabilization of complexes by use of cholesterol-conjugated siRNA. (A) The portion of siRNA dissociated from TEPA-PCL by PEGylation was separated by gel electrophoresis and stained with ethidium bromide. (B) The interaction between TEPA-PCL and siRNA was improved by modifying siRNA with cholesterol at the 3'-prime of the sense strand. The portion of siRNA or siRNA-C dissociated from TEPA-PCL by PEGylation was visualized by a similar procedure. (C, D) RNAi efficiency of siRNA-C transfected with TEPA-PCL was determined. A549-luc-C8 (C) or B16-F10-luc2 (D) cells (5×10^3 cells/well) were precultured overnight. TEPA-PCL complexed with siRNA (siLuc, siLuc-C; 10 pmol, N/P = 18 equiv (C), siCont-C, or siLuc2-C, 20 pmol, N/P = 18 equiv (D)) was added to these cells and removed after a 24 h incubation. These cells were subsequently cultured for additional 24 h and used for the luciferase assay. B16-F10-luc2 cells were also transfected with siLuc2 mixed with LFA2K according to the manufacturer's instructions. The control is that of cells not transfected with siRNA. Data are presented as the percentage of control luminescence intensity.

clearance from the bloodstream. The biodistribution of TEPA-PCL modified with 10% PEG2000 was almost similar to that of TEPA-PCL without PEG. On the other hand, TEPA-PCL modified with 20% PEG2000 avoided RES uptake and showed long-term circulation in the bloodstream. The length of PEG on TEPA-PCL also affected the avoidance of PEGylated TEPA-PCL from the RES uptake. TEPA-PCL modified with PEG6000 avoided RES uptake and showed long-term circulation in the bloodstream even when the percent molar ratio of DSPE-PEG to total lipids was 10%. The long-term circulation property of

TEPA-PCL modified with PEG6000 was superior to that with PEG2000. On the basis of these data, TEPA-PCL modified with 10% PEG6000 was adopted for subsequent experiments.

Stabilization of Complexes by Use of Cholesterol-Conjugated siRNA. Complex formation of PEGylated TEPA-PCL/siRNA was examined by electrophoresis in 15% acrylamide gels. As a result, free siRNA dissociated from TEPA-PCL was detected after PEGylation (Figure 3A). In contrast, siRNA was stably associated to TEPA-PCL by modifying the siRNA with cholesterol at the 3'-prime of the sense strand (Figure 3B). In the case of TEPA-PCL/siRNA-C complexes, free siRNA-C was not detected when they were formed at an N/P ratio of 18−30. In contrast, free siRNA dissociated from TEPA-PCL/siRNA complexes at all N/P ratios tested. The influence of cholesterol-conjugation on siRNA on knockdown efficiency was examined by using A549-luc-C8 cells and siLuc-C. TEPA-PCL complexed with siLuc or siLuc-C was used to transfect A549-luc-C8 cells. As a result, cholesterol-conjugation at the 3'-prime end of the sense strand of the siRNA did not affect the knockdown efficiency (Figure 3C). The knockdown efficiency of TEPA-PCL was also examined in another experimental model using B16−F10-luc2 cells and siLuc2-C. The knockdown efficiency of TEPA-PCL/siLuc2-C was higher than that obtained with LFA2K (Figure 3D).

NIRF Imaging of siRNA in Tumor-Bearing Mice. The biodistribution of AF750-siCont-C after intravenous injection in Colon26 NL-17 carcinoma-bearing mice was imaged *in vivo* by use of IVIS (Figure 4A). *In vivo* imaging data showed that fluorescent signals of AF750 were observed in the whole body of all mice at 10 min and 3 h after the injection. Accumulation of AF750 in the bladder was also observed in all groups up to 24 h after the injection. The total fluorescence of AF750 injected with TEPA-PCL was stronger than that without TEPA-PCL at 24 h after the injection. Importantly, AF750-siCont-C formulated in APRPG-TEPA-PCL accumulated in the tumor 24 h after the injection. *Ex vivo* images of each organ were obtained 96 h after the injection (Figure 4B). The total fluorescence of AF750 was low in siCont-C without TEPA-PCL. Accumulation of AF750 in the liver was observed with PEG-TEPA-PCL. In addition, strong fluorescent signals of AF750 in the tumor were observed only in the case of APRPG-TEPA-PCL.

■ **DISCUSSION**

Our previous results showed that siRNA formulated in cetyl-PEI-PCL showed efficient gene silencing in EGFP/HT-1080 cells and human umbilical vein endothelial cells.[17] However, cetyl-PEI-PCL modified with PEG6000 accumulated in the RES immediately after intravenous injection into mice. We considered that PEG6000 modification could not negate the undesirable properties of cetyl-PEI-PCL because of the molecular size of PEI[1800]. On the basis of these results, DCP-TEPA was newly synthesized and liposomalized for systemic siRNA delivery. Since TEPA is a relatively short polycation, we expected it to be stably presented on the liposomal membrane and not to interfere with the beneficial effects of PEGylation. In fact, PEG6000 endowed TEPA-PCL with the property of long circulation. On the other hand, we previously reported gene delivery with liposomal polyamine (spermidine, spermine, and PEI[1800])-dialkyl (dilauryl (DLP), dimyristyl (DMP), and DCP) phosphate conjugates.[14] Our previous results demonstrated that not only the polyamine but also the dialkyl parts affect their transfection efficiencies and that DCP is favorable for polyamine-mediated
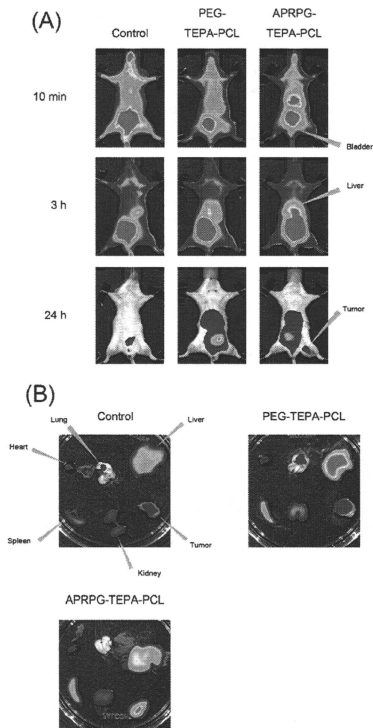
Figure 4. NIRF-imaging of APRPG-TEPA-PCL/AF750-siCont-C in tumor-bearing mice. (A, B) Colon26 NL-17 carcinoma-bearing BALB/c mice ($n = 3$) were intravenously injected with AF750-siCont-C (15 μg), PEG-TEPA-PCL/AF750-siCont-C or APRPG-TEPA-PCL/AF750-siCont-C (15 μg, N/P = 18 equiv) via the tail vein under anesthesia. The biodistribution of AF750-siCont-C was assessed with a Xenogen IVIS Lumina System coupled to *Living Image* software for data acquisition. (A) The fluorescence of AF750 in these mice was acquired *in vivo* 10 min, 3 h, and 24 h after the injection. (B) The fluorescence of AF750 in each organ (heart, lungs, liver, spleen, kidneys, and tumor) acquired *ex vivo* at 96 h after the injection.

gene delivery. For these reasons, we designed DCP-TEPA for systemic siRNA delivery.

In the present study, we first determined the formulation of TEPA-PCL/siRNA complexes by performing knockdown experiments. Interestingly, the amount of DCP-TEPA in PCL clearly affected the knockdown efficiency, but did not show dose dependency. This phenomenon might be related to the stability of TEPA-PCL, since the hydrophilic portion of DCP-TEPA relatively large compared with conventional liposomal components. Our data suggest that the amount of DCP-TEPA in TEPA-

PCL and the N/P ratio of TEPA-PCL/siRNA are important for gene silencing. On the other hand, PEGylation of TEPA-PCL/siRNA complexes caused dissociation of a part of siRNA from the TEPA-PCL, even though the formation of TEPA-PCL/siRNA complexes is based on electrostatic interactions. However, we could prevent this undesirable phenomenon by adding hydrophobic cholesterol to complexes by using siRNA-C. It is still not presently clear how DSPE-PEG removed siRNA from the TEPA-PCL. Modification of siRNA with cholesterol at the 3′-prime of the sense strand did not affect the knockdown efficiency, as previously reported.[10] Thus, modification of siRNA with certain compounds to improve the properties of nanoparticles could be a useful strategy and applicable to other situations. In addition, the transfection efficiency of TEPA-PCL/siRNA-C was higher than that of LFA2K. TEPA-PCL/siRNA-C would be internalized into cells by endocytosis and efficiently escape from endosomes possibly through the buffering effects, which have been observed in the case of cetyl-PEI[1800]-based PCL.[15]

The biodistribution study demonstrates that PEG6000 is suitable for PEGylation of TEPA-PCL. In general, the length of PEG2000 is adequate to endow neutral liposomes with long circulation. In fact, Doxil, which is a liposomal doxorubicin modified with MPEG2000, has such a property and is used worldwide as a cancer drug. In contrast, modification of TEPA-PCL with 10% PEG2000 did not alter the biodistribution of it after intravenous administration. This phenomenon might have been due to TEPA exposure on the liposomal surface despite PEGylation. Our data suggest that relatively long PEG chains would be needed to improve the biodistribution of positively charged liposomes in some cases. In addition, we modified PEGylated TEPA-PCL with APRPG for efficient delivery of siRNA into target cells since it is assumed that PEGylation of TEPA-PCL attenuates cellular uptake and gene silencing effects of siRNA formulated in TEPA-PCL. A steric barrier formed on the surface of liposomes by PEGylation is known to inhibit binding of liposomes to cells. In fact, our previous *in vitro* study using human umbilical vein endothelial cells revealed that PEGylation of cetyl-PEI-PCL attenuates cellular uptake of siRNA formulated in cetyl-PEI-PCL, whereas modification of PEGylated cetyl-PEI-PCL with APRPG improves this attenuation.[25]

In the NIRF imaging, we obtained not only *in vivo* but also *ex vivo* data, since the fluorescence intensities of *in vivo* NIRF imaging are strongly affected by tissue depth in animals.[18] As a result, both our *in vivo* and *ex vivo* data showed that AF750-siCont-C formulated in APRPG-TEPA-PCL accumulated in the tumor after intravenous injection into Colon26 NL-17 carcinoma-bearing mice. *In vivo* data also showed that the total fluorescent signals of AF750 observed in the whole body were almost similar between PEG-TEPA-PCL and APRPG-TEPA-PCL, suggesting that the presence of APRPG did not diminish the long-circulating property achieved by PEGylation. These data indicate that the accumulation of AF750-siCont-C formulated in APRPG-TEPA-PCL in the tumor would be achieved by both active targeting to angiogenic vessels and passive targeting by the EPR effect. These results are consistent with our previous results showing that modification of liposomes with APRPG-PEG conjugate should be useful for both drug and gene delivery to angiogenic vessels in tumors.[22,26−28]

In conclusion, we developed TEPA-PCL for efficient delivery of siRNA into tumor cells and angiogenic endothelial cells. Furthermore, we also developed APRPG-TEPA-PCL for targeting angiogenic vessels and achieved systemic delivery of siRNA to the tumors in *in vivo* study.

ARTICLE

■ ASSOCIATED CONTENT

Ⓢ Supporting Information. The ζ-potential of TEPA-PCL under various pH conditions (pH = approximately 4.1−7.9) was determined as an indicator of the buffering effects of TEPA in PCL and compared with that of 1,2-dioleoyl-3-trimethylammonium-propane (DOTAP) liposomes. The ζ-potential of TEPA-PCL under low pH conditions was higher than that under the neutral condition, whereas that of DOTAP liposomes did not change at any pH tested. This material is available free of charge via the Internet at http://pubs.acs.org.

■ AUTHOR INFORMATION

Corresponding Author
*Corresponding author. Tomohiro Asai, Department of Medical Biochemistry and Global COE, University of Shizuoka School of Pharmaceutical Sciences, 52-1 Yada, Suruga-ku, Shizuoka 422-8526, Japan. TEL: (81) 54 264 5703, FAX: (81) 54 264 5705. E-mail address: asai@u-shizuoka-ken.ac.jp.

■ ACKNOWLEDGMENT

■ REFERENCES

(1) Fire, A., Xu, S., Montgomery, M. K., Kostas, S. A., Driver, S. E., and Mello, C. C. (1998) Potent and specific genetic interference by double-stranded RNA in Caenorhabditis elegans. *Nature 391*, 806–811.

(2) Elbashir, S. M., Harborth, J., Lendeckel, W., Yalcin, A., Weber, K., and Tuschl, T. (2001) Duplexes of 21-nucleotide RNAs mediate RNA interference in cultured mammalian cells. *Nature 411*, 494–498.

(3) Sibley, C. R., Seow, Y., and Wood, M. J. (2010) Novel RNA-based strategies for therapeutic gene silencing. *Mol. Ther. 18*, 466–476.

(4) Tiemann, K., and Rossi, J. J. (2009) RNAi-based therapeutics-current status, challenges and prospects. *EMBO Mol. Med. 1*, 142–151.

(5) Manjunath, N., and Dykxhoorn, D. M. (2010) Advances in synthetic siRNA delivery. *Discovery Med. 9*, 418–430.

(6) Zimmermann, T. S., Lee, A. C., Akinc, A., Bramlage, B., Bumcrot, D., Fedoruk, M. N., Harborth, J., Heyes, J. A., Jeffs, L. B., John, M., Judge, A. D., Lam, K., McClintock, K., Nechev, L. V., Palmer, L. R., Racie, T., Rohl, I., Seiffert, S., Shanmugam, S., Sood, V., Soutschek, J., Toudjarska, I., Wheat, A. J., Yaworski, E., Zedalis, W., Koteliansky, V., Manoharan, M., Vornlocher, H. P., and MacLachlan, I. (2006) RNAi-mediated gene silencing in non-human primates. *Nature 441*, 111–114.

(7) Kim, S. H., Jeong, J. H., Lee, S. H., Kim, S. W., and Park, T. G. (2008) LHRH receptor-mediated delivery of siRNA using polyelectrolyte complex micelles self-assembled from siRNA-PEG-LHRH conjugate and PEI. *Bioconjugate Chem. 19*, 2156–2162.

(8) Chen, Y., Zhu, X., Zhang, X., Liu, B., and Huang, L. (2010) Nanoparticles modified with tumor-targeting scFv deliver siRNA and miRNA for cancer therapy. *Mol. Ther. 18*, 1650–1656.

(9) Li, J., Chen, Y. C., Tseng, Y. C., Mozumdar, S., and Huang, L. (2010) Biodegradable calcium phosphate nanoparticle with lipid coating for systemic siRNA delivery. *J. Controlled Release 142*, 416–421.

(10) Wolfrum, C., Shi, S., Jayaprakash, K. N., Jayaraman, M., Wang, G., Pandey, R. K., Rajeev, K. G., Nakayama, T., Charrise, K., Ndungo, E. M., Zimmermann, T., Koteliansky, V., Manoharan, M., and Stoffel, M. (2007) Mechanisms and optimization of in vivo delivery of lipophilic siRNAs. *Nat. Biotechnol. 25*, 1149–1157.

(11) Yamazaki, Y., Nango, M., Matsuura, M., Hasegawa, Y., Hasegawa, M., and Oku, N. (2000) Polycation liposomes, a novel nonviral

gene transfer system, constructed from cetylated polyethylenimine. *Gene Ther. 7*, 1148–1155.

(12) Oku, N., Yamazaki, Y., Matsuura, M., Sugiyama, M., Hasegawa, M., and Nango, M. (2001) A novel non-viral gene transfer system, polycation liposomes. *Adv. Drug Delivery Rev. 52*, 209–218.

(13) Dewa, T., Ieda, Y., Morita, K., Wang, L., MacDonald, R. C., Iida, K., Yamashita, K., Oku, N., and Nango, M. (2004) Novel polyamine-dialkyl phosphate conjugates for gene carriers. Facile synthetic route via an unprecedented dialkyl phosphate. *Bioconjugate Chem. 15*, 824–830.

(14) Dewa, T., Asai, T., Tsunoda, Y., Kato, K., Baba, D., Uchida, M., Sumino, A., Niwata, K., Umemoto, T., Iida, K., Oku, N., and Nango, M. (2010) Liposomal polyamine-dialkyl phosphate conjugates as effective gene carriers: chemical structure, morphology, and gene transfer activity. *Bioconjugate Chem. 21*, 844–852.

(15) Sugiyama, M., Matsuura, M., Takeuchi, Y., Kosaka, J., Nango, M., and Oku, N. (2004) Possible mechanism of polycation liposome (PCL)-mediated gene transfer. *Biochim. Biophys. Acta 1660*, 24–30.

(16) Matsuura, M., Yamazaki, Y., Sugiyama, M., Ori, H., Nango, M., and Oku, N. (2003) Polycation liposome-mediated gene transfer in vivo. *Biochim. Biophys. Acta 1612*, 136–143.

(17) Asai, T., Suzuki, Y., Matsushita, S., Yonezawa, S., Yokota, J., Katanasaka, Y., Ishida, T., Dewa, T., Kiwada, H., Nango, M., and Oku, N. (2008) Disappearance of the angiogenic potential of endothelial cells caused by Argonaute2 knockdown. *Biochem. Biophys. Res. Commun. 368*, 243–248.

(18) Hatanaka, K., Asai, T., Koide, H., Kenjo, E., Tsuzuku, T., Harada, N., Tsukada, H., and Oku, N. (2010) Development of double-stranded siRNA labeling method using positron emitter and its in vivo trafficking analyzed by positron emission tomography. *Bioconjugate Chem. 21*, 756–763.

(19) Klibanov, A. L., Maruyama, K., Torchilin, V. P., and Huang, L. (1990) Amphipathic polyethyleneglycols effectively prolong the circulation time of liposomes. *FEBS Lett. 268*, 235–237.

(20) Lasic, D. D., Martin, F. J., Gabizon, A., Huang, S. K., and Papahadjopoulos, D. (1991) Sterically stabilized liposomes: a hypothesis on the molecular origin of the extended circulation times. *Biochim. Biophys. Acta 1070*, 187–192.

(21) Maeda, H., Wu, J., Sawa, T., Matsumura, Y., and Hori, K. (2000) Tumor vascular permeability and the EPR effect in macromolecular therapeutics: a review. *J. Controlled Release 65*, 271–284.

(22) Asai, T., Miyazawa, S., Maeda, N., Hatanaka, K., Katanasaka, Y., Shimizu, K., Shuto, S., and Oku, N. (2008) Antineovascular therapy with angiogenic vessel-targeted polyethyleneglycol-shielded liposomal DPP-CNDAC. *Cancer Sci. 99*, 1029–1033.

(23) Yamakawa, S., Furuyama, Y., and Oku, N. (2000) Development of a simple cell invasion assay system. *Biol. Pharm. Bull. 23*, 1264–1266.

(24) Oku, N., Doi, K., Namba, Y., and Okada, S. (1994) Therapeutic effect of adriamycin encapsulated in long-circulating liposomes on Meth-A-sarcoma-bearing mice. *Int. J. Cancer 58*, 415–419.

(25) Hatanaka, K., Shimizu, K., Asai, T., and Oku, N. (2008) Antineovascular gene therapy by ago2 knockdown. *Yakugaku Zasshi 128*, 1567–1575.

(26) Oku, N., Asai, T., Watanabe, K., Kuromi, K., Nagatsuka, M., Kurohane, K., Kikkawa, H., Ogino, K., Tanaka, M., Ishikawa, D., Tsukada, H., Momose, M., Nakayama, J., and Taki, T. (2002) Antineovascular therapy using novel peptides homing to angiogenic vessels. *Oncogene 21*, 2662–2669.

(27) Yonezawa, S., Asai, T., and Oku, N. (2007) Effective tumor regression by anti-neovascular therapy in hypovascular orthotopic pancreatic tumor model. *J. Controlled Release 118*, 303–309.

(28) Maeda, N., Miyazawa, S., Shimizu, K., Asai, T., Yonezawa, S., Kitazawa, S., Namba, Y., Tsukada, H., and Oku, N. (2006) Enhancement of anticancer activity in antineovascular therapy is based on the intratumoral distribution of the active targeting carrier for anticancer drugs. *Biol. Pharm. Bull. 29*, 1936–1940.

Suppression of Choroidal Neovascularization by Intravitreal Injection of Liposomal SU5416

Miki Honda, MD; Tomohiro Asai, PhD; Takuya Umemoto, MS;
Yoshihiko Araki, MD; Naoto Oku, PhD; Minoru Tanaka, MD

Objective: To clarify whether use of angiogenic vessel-homing peptide, Ala-Pro-Arg-Pro-Gly (APRPG)– modified liposomes encapsulating 3-([2,4-dimethylpyrrhol-5-yl] methylidenyl)-indolin-2-one (SU5416), an angiogenesis inhibitor, can inhibit the development of experimental choroidal neovascularization (CNV) in rats.

Methods: Liposomes were prepared using the thin-film hydration method. To set up the rat experimental CNV model, intense fundus laser photocoagulation at 6 spots per eye was performed on pigmented rats. After photocoagulation, the rats were divided into 4 groups (6 rats in each group): an APRPG-liposomal SU5416 treatment group and control groups treated with a balanced salt solution, APRPG liposomes, or soluble SU5416. Each rat received a single intravitreal injection immediately after the injury. One week or 2 weeks after laser injury, the extent of CNV was evaluated by perfu-

sion with high-molecular-weight fluorescein isothiocyanate-dextran.

Results: Two weeks after injection, the CNV area was significantly ($P<.05$) smaller in the APRPG-liposomal SU5416–treated group compared with the CNV area in the balanced salt solution– and APRPG liposome–treated groups.

Conclusion: Liposomes modified by APRPG and encapsulating SU5416 constitute a potential drug formulation for CNV treatment that would require only a single intravitreal injection.

Clinical Relevance: This liposomal delivery may enable the sustained release of small molecules and be a new treatment modality for CNV.

Arch Ophthalmol. 2011;129(3):317-321

Author Affiliations:
Department of Ophthalmology, Juntendo University Urayasu Hospital, Chiba, Japan (Drs Honda and Tanaka); Department of Medical Biochemistry, School of Pharmaceutical Sciences, University of Shizuoka, Shizuoka, Japan (Drs Asai and Oku and Ms Umemoto); Institute for Environmental and Gender-Specific Medicine, Juntendo University Graduate School of Medicine, Chiba, Japan (Dr Araki).

CHOROIDAL NEOVASCULAR-ization (CNV) is a key pathologic change, causing severe vision loss as part of the pathogenesis of several diseases. The most prevalent disease of this type is exudative age-related macular degeneration (AMD), resulting in irreversible vision loss, which primarily affects people in developed countries.[1,2] In relation to pathomorphologic disorders, various angiogenic growth factors, including vascular endothelial growth factor (VEGF), have been reported[3-5] to be expressed in CNV tissue and in retinal pigment epithelium (RPE) cells. Vascular endothelial growth factor is believed to be one of the major regulators in a variety of physiologic and pathologic angiogenesis processes, including CNV.[6-9] In addition, the molecular expression of VEGF and its receptors (VEGFRs) is upregulated in rat experimental CNV models.[5,10]

Two types of endothelium-specific tyrosine kinase receptors, Flt-1 (VEGFR1) and KDR/Flk-1 (VEGFR2), are known to

mediate the function of VEGF, as receptor molecules, in physiologic and pathologic neovascularization.[11-13] In addition, VEGFR2 is thought to mediate VEGF-induced signals such as vascular hyperpermeability and most angiogenic properties, including mitogenicity/chemotactic activity.[14]

To date, 2 antiangiogenic therapies have been approved for the treatment of exudative AMD: pegaptanib sodium, an oligonucleotide (Macugen; Eyetech Pharmaceuticals/Pfizer, New York, New York), and ranibizumab, an anti-VEGF antibody Fab fragment (Lucentis; Genentech/Novartis, Basel, Switzerland). Another VEGF blocker in ongoing clinical studies is VEGF trap, a fusion protein of domain 2 from VEGFR1 and domain 3 from VEGFR2. This recombinant fusion protein has a high affinity for VEGF and interacts with all VEGF isoforms as well as placental growth factors. All clinical trials to date have demonstrated satisfactory results with intravitreal delivery of these agents in patients with AMD. However,

there are serious clinical problems with these approaches. The desired therapeutic outcome often requires frequent injections. Repeated ocular injections are generally accompanied by risk of endophthalmitis, retinal detachment, and vitreous hemorrhage. Therefore, drug formulations, and especially drug delivery systems (DDSs), need to be improved to reduce the frequency of intravitreal injection. Vascular endothelial growth factor signal transduction inhibitors have been also used as antiangiogenic factors in chemotherapy. For example, sunitinib (Sutent, SU11248, Pfizer), a small molecule inhibitor of receptor tyrosine kinases of VEGFR and platelet-derived growth factor receptor, has been approved for the treatment of cancer.[15] The antiangiogenic compound SU5416 (3-[(2,4-dimethylpyrrhol-5-yl) methyl-idenyl]-indolin-2-one) is a potent and selective inhibitor of VEGFR2.[16] It has been shown[17] to suppress VEGF-mediated angiogenesis in vitro and in vivo through the inhibition of autophosphorylation of VEGFR2 by blocking the adenosine monophosphate–binding site within the kinase domain. In contrast to the successful results of phase 1 and 2 trials for the treatment of advanced cancers, SU5416 did not show any significant clinical benefit, and some patients experienced severe toxic reactions to the solvent used for dissolving SU5416, polyethoxylated castor oil.[18]

It has been demonstrated[19] that the liposomal formulation of SU5416 does not require polyethoxylated castor oil for administration. Furthermore, a liposomal DDS using the angiogenic vessel-homing peptide Ala-Pro-Arg-Pro-Gly (APRPG) for active targeting of the drug carrier to the angiogenic site was useful in the treatment of tumor-bearing mice.[20-22] Thus, this chemical compound is expected to be a new drug for treatment of AMD if an appropriate and safe DDS is developed.

Liposomes are small lipid vesicles and one of the most advanced drug nanocarriers in DDS studies.[23] The use of liposomal vehicles to prolong clearance and limit peak concentration after intravitreal injection might avert the risks of frequent intravitreal injections.[24] The aim of the present study was to clarify whether SU5416 can be applied in CNV treatment using a liposomal DDS.

METHODS

ANIMALS

Sexually mature male Brown Norway rats (weight, 180-200 g; Japan SLC, Inc, Shizuoka, Japan) were maintained under 12-hour light and 12-hour dark conditions and fed a standard rat chow and water ad libitum. All experiments adhered to the Association for Research in Vision and Ophthalmology Statement for the Use of Animals in Ophthalmic and Vision Research[25] and Juntendo University's guidelines for care and use of laboratory animals.

PREPARATION OF LIPOSOMAL SU5416

Liposomes were prepared as previously described.[21] In brief, DPPC (dipalmitoylphosphatidylcholine), POPC (palmitoyl-oleoylphosphatidylcholine), cholesterol, and SU5416 solutions in chloroform were mixed (10:10:5:1 molar ratio) and dried under reduced pressure to make a thin lipid film. The APRPG peptide-conjugated DSPE-PEG (distearoylphosphatidylethanolamine-polyethylene glycol) solution was added to the initial lipid solutions in the proportion of 10 mole percent (mol%) to phosphatidylcholine to modify the liposomes. For histochemical analysis, $DiIC_{18}$ (Molecular Probes, Inc, Eugene, Oregon) was added to the initial lipid solutions in the proportion of 10 mol% to phosphatidylcholine. The thin lipid films were hydrated with 20mM HEPES (2-[4-(2-hydroxyethyl)-1-piperazinyl]ethanesulfonic acid)–buffered saline (pH 7.4), and the liposome solutions underwent 3 freeze-thaw cycles using liquid nitrogen. The size of the liposomes was then adjusted by extruding through a 100-nm pore polycarbonate filter. The particle size and zeta potential of liposomal SU5416 were measured (Zetasizer; Malvern Instruments, Malvern, Worcestershire, England), and these values were approximately 130 nm and –2 mV, respectively.

INDUCTION OF CNV

Laser-induced CNV is widely used as an animal model for exudative AMD.[26] Using this model, we observed new vessels from the choroid that invaded the subretinal space after photocoagulation. Laser photocoagulation was performed in 6 spots per eye around the optic disc (wavelength, 532 nm; power, 90 mW; spot diameter, 100 µm) using a slit delivery system (NOVUS Spectra; Lumenis, Tokyo, Japan), as described.[27,28] After photocoagulation, the rats were divided into 4 experimental groups (6 rats in each group) and were given APRPG-liposomal SU5416, balanced salt solution (BSS), APRPG liposomes, or soluble SU5416 for administration of the drug. The SU5416 concentration used was 0.625 mg/mL. Immediately after photocoagulation, each rat received a single 10-µL intravitreal injection using a 30-gauge needle.

VISUALIZING AND QUANTIFYING CNV

One week or 2 weeks after injury, blood flow was visualized by vascular perfusion with high-molecular-weight (2×10^6–MW [2-MMW]) fluorescein isothiocyanate (FITC)–dextran (Sigma-Aldrich Corp, St Louis, Missouri) using the method described by D'Amato et al.[29] Briefly, animals were anesthetized with intraperitoneal injection of sodium pentobarbital, 30 mg (Nembutal; Dainippon Sumitomo Pharma Co, Ltd, Osaka, Japan) per kilogram of body weight. The left ventricle was then perfused with approximately 50 mL of lactated Ringer solution, followed with 20 mL of lactated Ringer solution containing 10% (wt/vol) gelatin and 5-mg/mL FITC-dextran. After perfusion, treated eyes were enucleated and fixed with 4% paraformaldehyde solution for 20 minutes. Retinal pigment epithelium–choroid-sclera flat mounts were obtained by hemisecting the eye and peeling the neural retina away from the underlying RPE. Radial cuts allowed the eyecup to be laid flat onto a microscope slide with the RPE side facing up. Flat mounts were fixed by mounting medium (Vectashield; Vector Laboratories, Inc, Burlingame, California), and the specimens were examined with a microscope (Biorevo BZ-9000; Keyence, Osaka, Japan) equipped with an FITC-detecting filter unit. The CNV areas were photographed with a charge-coupled device camera and captured with an image analysis system (BZ-II; Keyence). The FITC-dextran–perfused vessels representing neovascularization were quantified by an experienced clinician (M.H.) delineating the perimeter of the fibrovascular membranes.

ACCUMULATION OF FLUORESCEIN LIPOSOMAL SU5416 IN CNV

To investigate the accumulation of APRPG-liposomal SU5416 in CNV, double-labeling experiments including $DiIC_{18}$ (red fluo-
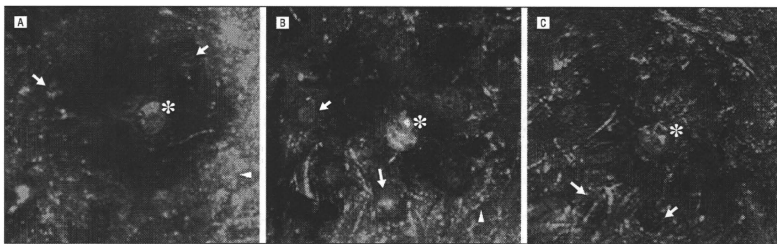
Figure 1. Liposomal SU5416 (3-[(2,4-dimethylpyrrhol-5-yl) methylidenyl]-indolin-2-one) (red) and choroidal vascularization (green) double labeling. Localization of (Ala-Pro-Arg-Pro-Gly [APRPG]–free) liposomal SU5416 (A) and APRPG-liposomal SU5416 (B) 4 days after intravitreal injection, as well as APRPG-liposomal SU5416 at 2 weeks after injection (C). Asterisks indicate optic nerve; arrows, choroidal neovascularization region; arrowheads, normal choroidal vessels.

rescence) were performed. Just after laser injury, (APRPG-free) liposomal SU5416 and APRPG-liposomal SU5416 were intravitreally injected in rats. Four days or 2 weeks after injection, the accumulation of liposomal SU5416 in choroidal flatmount was examined using an epifluorescent microscope.

STATISTICAL ANALYSIS

Experimental results of the quantitative analysis are expressed as the mean (SE). Data were analyzed by analysis of variance with the Tukey test. A probability of $P < .05$ was considered statistically significant.

RESULTS

To evaluate the effect of vascular-targeted liposomal SU5416 on CNV, the morphologic effect of the compound was examined by angiography using 2-MMW FITC-dextran and by epifluorescent microscopy. The rat experimental model was chosen for this study to determine the pharmacologic effect of the liposomal chemical compound on CNV, since this animal model of laser-induced CNV has been widely used[30,31] in the evaluation of experimental AMD treatments. The rat model of laser-induced CNV has a high reproducibility.

As an initial experiment, we examined the accumulation of liposomal SU5416 after intravitreal injection by using DiIC$_{18}$ (red fluorescence) to clarify whether the efficacy of liposomal SU5416 might be enhanced by the angiogenic-homing peptide (APRPG) or only by sustained release from liposomes. Four days after laser injury and intravitreal injection, significant amounts of APRPG-liposomal SU5416 recruited to the developing CNV region were compared with the control (APRPG-free liposomal SU5416) (**Figure 1**A and B). The APRPG-liposomal SU5416 remained in the CNV region 2 weeks after intravitreal injection (Figure 1C).

The typical CNV observed by fluorescent microscopy in the present study is shown in **Figure 2**. Two weeks after the injury, CNV was observed as relative hyperfluorescence areas overlying the laser lesions in the RPE-choroid-sclera flat mounts. Although CNV in the group treated with soluble SU5416 appeared to be somewhat inhibited (Figure 2C), the inhibitory effects on the induced CNV were enhanced when the animals
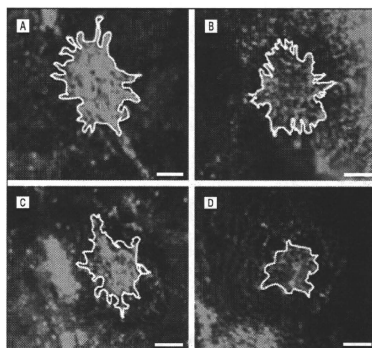

Figure 2. Morphologic changes of laser-induced choroidal neovascularization (CNV) after intravitreal injection. Typical fluorescein angiogram of retinal pigment epithelium 2 weeks after injury treated with balanced salt solution (A), Ala-Pro-Arg-Pro-Gly (APRPG) liposomes (B), soluble SU5416 (3-[(2,4-dimethylpyrrhol-5-yl) methylidenyl]-indolin-2-one) (C), or APRPG peptide-modified liposomal SU5416 (D). Regions of CNV are outlined by a solid line. Bars represent 100 μm.

were treated with APRPG peptide-modified liposomal SU5416 (Figure 2D) compared with the controls (Figure 2A and B).

Attempts were then made to quantify the analysis by measuring the CNV areas in images of each experimental group. One week after laser injury and intravitreal injection, neovascular regions in RPE showed that the area of CNV in the soluble SU5416-treated group (19 598 [1128] μm^2) was significantly smaller than that in each of the other 2 groups (BSS, 25 092 [1584] μm^2; APRPG liposomes, 24 987 [1641] μm^2). No significant difference was observed between the group treated with APRPG-liposomal SU5416 (20 177 [1339] μm^2) and each of the other control groups (BSS and APRPG liposomes) (**Figure 3**A).

Data obtained from traced neovascular regions in RPE 2 weeks after injury showed that the area of CNV in the APRPG-liposomal SU5416–treated group (28 431 [2237]
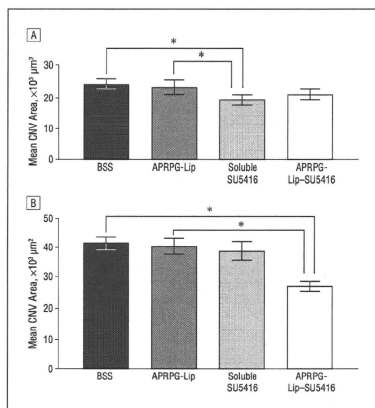
Figure 3. Quantitative analysis of the choroidal neovascularization (CNV) area in each experimental group 1 week (A) and 2 weeks (B) after intravitreal injection. The results are expressed as simple mean (SE) of CNV area (n=6). *Statistical significance between indicated groups at $P < .05$. APRPG-Lip indicates Ala-Pro-Arg-Pro-Gly–modified liposomes; BSS, balanced salt solution; and SU5416, 3-([2,4-dimethylpyrrhol-5-yl] methylidenyl)-indolin-2-one.

μm^2) was significantly smaller than that in each of the other 2 groups (BSS and APRPG liposomes). However, no significant difference was observed between the group treated with soluble SU5416 (38 160 [3550] μm^2) and that treated with APRPG liposomes (40 788 [2845] μm^2) or BSS (421 437 [2468] μm^2) (Figure 3B).

COMMENT

The data from this study clearly demonstrate that a single intravitreal injection of the vascular-targeted liposomal SU5416 significantly reduced laser-induced CNV in the experimental rat model. This implies that the liposomal compound may be useful in the treatment of CNV in clinical practice via its inhibitory effect on VEGF. Indeed, intravitreal injections using liposomal chemicals such as antibiotics (clindamycin,[32,33] gentamicin,[34] and amikacin[35]), a polyene antifungal (amphotericin B[36,37]), an immunosuppressant (cyclosporine[38]), and antimetabolites (fluorouracil, fluorouridine[39,40]) have been reported to be effective.

SU5416 inhibits the phosphorylation of VEGFR2 in a dose-dependent manner in vitro.[18] It is assumed that SU5416 inhibits neovascularization by blocking VEGFR2 downstream signal transduction in vivo. Previous animal model studies on SU5416 demonstrated its tumor-suppressive effect. For example, a 73% decrease in tumor volume has been demonstrated[18] by SU5416 administration in a null/null mouse model after rat C6 glioma cells were transplanted into the colon serosa. The inhibition of VEGFR2 phosphorylation by in-

traperitoneal injection of SU5416 once daily for 2 weeks has been shown in the rat model, and SU5416 also showed a tumor-suppressive effect in a rat experimental CNV model.[41] In addition, apoptosis has been induced in murine CNV endothelial cells after administration of SU5416 by intraperitoneal injection every other day for 14 days.[28]

Treatment using soluble SU5416 inhibited CNV development 1 week (but not 2 weeks) after injection compared with APRPG-liposomal SU5416 (Figure 3). Because APRPG-liposomal SU5416 was observed at the CNV region 2 weeks after intravitreal injection (Figure 1C), these results suggest that APRPG-liposomal SU5416 has a long-standing effect for CNV reduction.

Based on the inhibitory effects of SU5416 on CNV in vivo, the present study evaluated the validity of a novel DDS—a single intravitreal injection of an angiogenic vessel-homing peptide, APRPG—for the active targeting of drug carriers to angiogenic sites. Healthy choroidal vessels in the APRPG-liposomal SU5416–treated group were not noted (Figure 2). However, Shimotake et al[42] recently reported that VEGF inhibition could affect normal vessels as well as angiogenic vessels; further studies concerning the effect of liposomal SU5416 on healthy tissues are necessary to clarify the issue.

We believe that the liposomal DDS provided significant basic data for clinical use for the following reasons: (1) the efficiency of the liposomal method used in this study was satisfactory for use in an in vivo study, (2) it is believed that APRPG-liposomal SU5416 may be stable in the vitreous humor, and (3) APRPG has been reported[21] in studies of tumor therapies to be effective in active targeting of drug carriers to angiogenic sites in the vitreous body.

Although further investigation of the precise mechanism and direct molecular basis of the effect of vitreous injection of APRPG-liposomal SU5416 on CNV inhibition is necessary, the findings in this study suggest that APRPG-liposomal SU5416 is a strong candidate for development as an agent for the treatment of conditions such as exudative AMD by a single vitreous injection. The liposomal delivery of small compounds may be a new treatment modality for CNV.

REFERENCES

1. Lee P, Wang CC, Adamis AP. Ocular neovascularization: an epidemiologic review. *Surv Ophthalmol*. 1998;43(3):245-269.
2. Leibowitz HM, Krueger DE, Maunder LR, et al. The Framingham Eye Study monograph: an ophthalmological and epidemiological study of cataract, glaucoma, diabetic retinopathy, macular degeneration, and visual acuity in a general population of 2631 adults, 1973-1975. *Surv Ophthalmol*. 1980;24(suppl):335-610.
3. Ishibashi T, Hata Y, Yoshikawa H, Nakagawa K, Sueishi K, Inomata H. Expression of vascular endothelial growth factor in experimental choroidal neovascularization. *Graefes Arch Clin Exp Ophthalmol*. 1997;235(3):159-167.
4. Lopez PF, Sippy BD, Lambert HM, Thach AB, Hinton DR. Transdifferentiated retinal pigment epithelial cells are immunoreactive for vascular endothelial growth factor in surgically excised age-related macular degeneration-related choroidal neovascular membranes. *Invest Ophthalmol Vis Sci*. 1996;37(5):855-868.
5. Yi X, Ogata N, Komada M, et al. Vascular endothelial growth factor expression in choroidal neovascularization in rats. *Graefes Arch Clin Exp Ophthalmol*. 1997; 235(5):313-319.
6. Amin R, Puklin JE, Frank RN. Growth factor localization in choroidal neovascular membranes of age-related macular degeneration. *Invest Ophthalmol Vis Sci*. 1994;35(8):3178-3188.
7. Carmeliet P, Ferreira V, Breier G, et al. Abnormal blood vessel development and lethality in embryos lacking a single VEGF allele. *Nature*. 1996;380(6573):435-439.
8. Folkman J. Angiogenesis in cancer, vascular, rheumatoid and other disease. *Nat Med*. 1995;1(1):27-31.
9. Kvanta A. Expression and regulation of vascular endothelial growth factor in choroidal fibroblasts. *Curr Eye Res*. 1995;14(11):1015-1020.
10. Wada M, Ogata N, Otsuji T, Uyama M. Expression of vascular endothelial growth factor and its receptor (KDR/flk-1) mRNA in experimental choroidal neovascularization. *Curr Eye Res*. 1999;18(3):203-213.
11. de Vries C, Escobedo JA, Ueno H, Houck K, Ferrara N, Williams LT. The fms-like tyrosine kinase, a receptor for vascular endothelial growth factor. *Science*. 1992; 255(5047):989-991.
12. Millauer B, Wizigmann-Voos S, Schnürch H, et al. High affinity VEGF binding and developmental expression suggest Flk-1 as a major regulator of vasculogenesis and angiogenesis. *Cell*. 1993;72(6):835-846.
13. Waltenberger J, Claesson-Welsh L, Siegbahn A, Shibuya M, Heldin CH. Different signal transduction properties of KDR and Flt1, two receptors for vascular endothelial growth factor. *J Biol Chem*. 1994;269(43):26988-26995.
14. Wu LW, Mayo LD, Dunbar JD, et al. Utilization of distinct signaling pathways by receptors for vascular endothelial cell growth factor and other mitogens in the induction of endothelial cell proliferation. *J Biol Chem*. 2000;275(7):5096-5103.
15. Spannuth WA, Sood AK, Coleman RL. Angiogenesis as a strategic target for ovarian cancer therapy. *Nat Clin Pract Oncol*. 2008;5(4):194-204.
16. Fong TA, Shawver LK, Sun L, et al. SU5416 is a potent and selective inhibitor of the vascular endothelial growth factor receptor (Flk-1/KDR) that inhibits tyrosine kinase catalysis, tumor vascularization, and growth of multiple tumor types. *Cancer Res*. 1999;59(1):99-106.
17. Mendel DB, Schreck RE, West DC, et al. The angiogenesis inhibitor SU5416 has long-lasting effects on vascular endothelial growth factor receptor phosphorylation and function. *Clin Cancer Res*. 2000;6(12):4848-4858.
18. Ye C, Sweeny D, Sukbuntherng J, et al. Distribution, metabolism, and excretion of the anti-angiogenic compound SU5416. *Toxicol In Vitro*. 2006;20(2):154-162.
19. Katanasaka Y, Ida T, Asai T, et al. Antiangiogenic cancer therapy using tumor vasculature-targeted liposomes encapsulating 3-(3,5-dimethyl-1H-pyrrol-2-ylmethylene)-1,3-dihydro-indol-2-one, SU5416. *Cancer Lett*. 2008;270(2):260-268.
20. Maeda N, Miyazawa S, Shimizu K, et al. Enhancement of anticancer activity in antineovascular therapy is based on the intratumoral distribution of the active targeting carrier for anticancer drugs. *Biol Pharm Bull*. 2006;29(9):1936-1940.
21. Maeda N, Takeuchi Y, Takada M, Sadzuka Y, Namba Y, Oku N. Anti-neovascular therapy by use of tumor neovasculature-targeted long-circulating liposome. *J Control Release*. 2004;100(1):41-52.
22. Oku N, Asai T, Watanabe K, et al. Anti-neovascular therapy using novel peptides homing to angiogenic vessels. *Oncogene*. 2002;21(17):2662-2669.
23. Allen TM, Cullis PR. Drug delivery systems: entering the mainstream. *Science*. 2004;303(5665):1818-1822.
24. Ebrahim S, Peyman GA, Lee PJ. Applications of liposomes in ophthalmology. *Surv Ophthalmol*. 2005;50(2):167-182.
25. Demers G, Griffin G, De Vroey G, Haywood JR, Zurlo J, Bédard M. Animal research: harmonization of animal care and use guidance. *Science*. 2006;312 (5774):700-701.
26. Takehana Y, Kurokawa T, Kitamura T, et al. Suppression of laser-induced choroidal neovascularization by oral tranilast in the rat. *Invest Ophthalmol Vis Sci*. 1999;40(2):459-466.
27. Edelman JL, Castro MR. Quantitative image analysis of laser-induced choroidal neovascularization in rat. *Exp Eye Res*. 2000;71(5):523-533.
28. Kami J, Muranaka K, Yanagi Y, Obata R, Tamaki Y, Shibuya M. Inhibition of choroidal neovascularization by blocking vascular endothelial growth factor receptor tyrosine kinase. *Jpn J Ophthalmol*. 2008;52(2):91-98.
29. D'Amato R, Wesolowski E, Smith LE. Microscopic visualization of the retina by angiography with high-molecular-weight fluorescein-labeled dextrans in the mouse. *Microvasc Res*. 1993;46(2):135-142.
30. Zacks DN, Ezra E, Terada Y, et al. Verteporfin photodynamic therapy in the rat model of choroidal neovascularization: angiographic and histologic characterization. *Invest Ophthalmol Vis Sci*. 2002;43(7):2384-2391.
31. Ciulla TA, Criswell MH, Danis RP, Hill TE. Intravitreal triamcinolone acetonide inhibits choroidal neovascularization in a laser-treated rat model. *Arch Ophthalmol*. 2001;119(3):399-404.
32. Fiscella R, Peyman GA, Fishman PH. Duration of therapeutic levels of intravitreally injected liposome-encapsulated clindamycin in the rabbit. *Can J Ophthalmol*. 1987;22(6):307-309.
33. Rao VS, Peyman GA, Khoobehi B, Vangipuram S. Evaluation of liposome-encapsulated clindamycin in *Staphylococcus aureus* endophthalmitis. *Int Ophthalmol*. 1989;13(3):181-185.
34. Fishman PH, Peyman GA, Lesar T. Intravitreal liposome-encapsulated gentamicin in a rabbit model: prolonged therapeutic levels. *Invest Ophthalmol Vis Sci*. 1986;27(7):1103-1106.
35. Zeng S, Hu C, Wei H, et al. Intravitreal pharmacokinetics of liposome-encapsulated amikacin in a rabbit model. *Ophthalmology*. 1993;100(11):1640-1644.
36. Tremblay C, Barza M, Szoka F, Lahav M, Baum J. Reduced toxicity of liposome-associated amphotericin B injected intravitreally in rabbits. *Invest Ophthalmol Vis Sci*. 1985;26(5):711-718.
37. Liu KR, Peyman GA, Khoobehi B. Efficacy of liposome-bound amphotericin B for the treatment of experimental fungal endophthalmitis in rabbits. *Invest Ophthalmol Vis Sci*. 1989;30(7):1527-1534.
38. Alghadyan AA, Peyman GA, Khoobehi B, Milner S, Liu KR. Liposome-bound cyclosporine: clearance after intravitreal injection. *Int Ophthalmol*. 1988;12(2):109-112.
39. Joondeph BC, Peyman GA, Khoobehi B, Yue BY. Liposome-encapsulated 5-fluorouracil in the treatment of proliferative vitreoretinopathy. *Ophthalmic Surg*. 1988; 19(4):252-256.
40. Fishman P, Peyman GA, Hendricks R, Hui SL. Liposome-encapsulated 3H-5FU in rabbits. *Int Ophthalmol*. 1989;13(5):361-365.
41. Takeda A, Hata Y, Shiose S, et al. Suppression of experimental choroidal neovascularization utilizing KDR selective receptor tyrosine kinase inhibitor. *Graefes Arch Clin Exp Ophthalmol*. 2003;241(9):765-772.
42. Shimotake J, Derugin N, Wendland M, Vexler ZS, Ferriero DM. Vascular endothelial growth factor receptor-2 inhibition promotes cell death and limits endothelial cell proliferation in a neonatal rodent model of stroke. *Stroke*. 2010; 41(2):343-349.

Contents lists available at ScienceDirect

International Journal of Pharmaceutics

Pharmaceutical Nanotechnology

PET imaging of brain cancer with positron emitter-labeled liposomes

Naoto Oku [a,*], Mina Yamashita [a], Yurie Katayama [a], Takeo Urakami [a,1], Kentaro Hatanaka [a], Kosuke Shimizu [a], Tomohiro Asai [a], Hideo Tsukada [b], Shuji Akai [c], Hiroaki Kanazawa [d]

[a] Department of Medical Biochemistry and Global COE, Graduate School of Pharmaceutical Sciences, University of Shizuoka, Yada, Suruga-ku, Shizuoka 422-8526, Japan
[b] PETCenter, Central Research Laboratory, Hamamatsu Photonics K.K. Hirakuchi, Hamakita-ku, Hamamatu, Shizuoka 434-8601, Japan
[c] Department of Synthetic Organic Chemistry, Graduate School of Pharmaceutical Sciences, University of Shizuoka, Yada, Suruga-ku, Shizuoka 422-8526, Japan
[d] Department of Anatomy, School of Nursing, University of Shizuoka, Yada, Suruga-ku, Shizuoka 422-8526, Japan

ARTICLE INFO

ABSTRACT

Since nanocarriers such as liposomes are known to accumulate in tumors of tumor-bearing animals, and those that have entrapped a positron emitter can be used to image a tumor by PET, we applied ^{18}F-labeled 100-nm-sized liposomes, which are known to accumulate in tumors of brain tumors. Polyethylene glycol (PEG)-modified liposomes, which are known to accumulate in tumors by passive targeting and those modified with Ala-Pro-Arg-Pro-Gly, which are known to home into angiogenic sites were used. Those liposomes labeled with DiI fluorescence accumulated in a glioma implanted in a rat brain 1 h after the injection, although they did not accumulate in the normal brain tissues due to the protection afforded by the blood–brain barrier. Preformed liposomes were easily labeled with 1-[18]fluoro-3,6-dioxatetracosane, and enabled the imaging of gliomas by PET with higher contrast than that obtained with [18]deoxyfluoroglucose. In addition, the smallest tumor among those tested, having a diameter of 1 mm was successfully imaged by the liposomal [18]F. Therefore, nanocarrier-based imaging of brain tumors is promising for the diagnosis of brain cancer and possible drug delivery-based therapy.

© 2010 Elsevier B.V. All rights reserved.

1. Introduction

Brain cancers such as glioblastomas are known to be aggressive and invasive (Wen and Kesari, 2008). Therefore, diagnosis of brain cancer at the early stages is quite important. Positron emission tomography (PET) is one of the strong tools for diagnosis, therapeutic evaluation, and prognostic evaluation of cancer. [2-^{18}F]-2-deoxyfluoro-D-glucose (FDG) is the most widely used positron emitter for cancer diagnosis (Scott et al., 2008; Nakamoto et al., 2009). However, the utility of FDG-PET imaging for detection of brain cancer is controversial due to the high demand for glucose in the brain (Takeda et al., 2003; Chen, 2007). To reduce this bothersome background various compounds such as [11C]choline (Tian et al., 2004; Kato et al., 2008), [11C]acetate (Yamamoto et al., 2008), and amino acid analogues such as [11C]methionine (Hatakeyama et al., 2008; Jager et al., 2001), L-[methyl-[11C]methionine (Nojiri et al., 2009; Ullrich et al., 2009), O-[11C]methyl-L-tyrosine (Ishiwata et al., 2004), O-[18F]fluoromethyl-L-tyrosine (Ishiwata et al., 2004),

O-[18F]fluoroethyl-L-tyrosine (Heiss et al., 1999; Langen et al., 2006; Floeth et al., 2007; Mehrkens et al., 2008; Pauleit et al., 2009), and O-[18F]fluoropropyl-L-tyrosine (Tang et al., 2003) have been synthesized and evaluated as PET imaging agents for the diagnosis and detection of recurrence of brain tumors. Among them, the amino acid analogues show relatively low accumulation in normal peripheral tissue (low tissue-to-blood ratio) and rapid blood clearance and have been used for detecting brain tumors and other tumors as well. We also demonstrated that the D-amino acid analogue O-[18F]fluoromethyl-D-tyrosine is useful for tumor imaging by PET (Urakami et al., 2009).

Nanomedicines such as liposomal drugs are known to accumulate in tumors due to the enhanced permeability of tumor blood vessels and the retention effect (Maeda et al., 2000, 2009). This drug delivery system (DDS) strategy is based on the nature of tumors: tumor cells demand oxygen and nutrition and cause angiogenesis for obtaining them, and angiogenic vessels are leaky enough to be permeated by nano-sized materials. Liposomes are known as one of the most effective drug carriers for cancer therapy. In liposomal DDS technologies, polyethylene glycol (PEG)-modified liposomes are useful drug carriers for cancer therapy; for they have a characteristically long circulation time in the bloodstream due to avoidance of being trapped by the reticuloendothelial system (RES) such as in the liver and spleen (Sakakibara et al., 1996;

* Corresponding author. Tel.: +81 54 264 5701; fax: +81 54 264 5705.
E-mail address: oku@u-shizuoka-ken.ac.jp (N. Oku).
[1] Present address: The Burnham Institute for Medical Research at Lake Nona, 6400 Sanger Rd., Orlando, FL 32827, United States.

Gabizon, 2001). PEG-modified liposomes tend to accumulate in tumor tissues through passive targeting, and PEG-modified liposomes containing doxorubicin have been used in clinical cancer therapy.

We previously demonstrated that PEG-liposomes encapsulating [18F]FDG accumulate in solid tumors and can be effectively imaged by PET (Oku et al., 1996). Although the encapsulation efficiency of [18F]FDG is not so high, the result indicated the usefulness of liposomes for cancer imaging. Moreover, actively targeting nanocarriers specifically associating with tumor cells or angiogenic vessels are an attractive approach. For example, we previously demonstrated that liposomes modified with a peptide specifically recognized by membrane type-1 matrix metalloproteinase (MT1-MMP), which is expressed on the surface of angiogenic endothelial cells, accumulate in tumors (Kondo et al., 2004). In that study, we encapsulated [18F]FDG in the liposomes and determined the distribution of the liposomes by PET. We also performed *in vivo* biopanning of a phage-displayed peptide library using an angiogenesis mouse model to obtain specific probes for angiogenic endothelial cells, and identified the Ala-Pro-Arg-Pro-Gly (APRPG) motif as a novel peptide homing to angiogenic vessels (Oku et al., 2002; Asai et al., 2002). Liposomes modified with APRPG and labeled with [3H]cholesterol hexadecylether actually accumulate in tumors of colon 26 NL-17 carcinoma-implanted mice (Maeda et al., 2004). Moreover, the accumulation of APRPG-modified liposomes in such tumors was also confirmed by PET analysis using [18F]FDG-encapsulated liposomes (Maeda et al., 2006).

In the present study, we applied PEG-modified and APRPG–PEG-modified liposomes entrapping a positron-emitter to brain tumor imaging by PET. At first, we analyzed distribution of fluorescence-labeled liposomes in glioma-bearing brain of rats by use of fluorescence microscopy and an *in vivo* fluorescence-based imaging system. Then PET imaging of brain cancers was achieved by use of 1-[18F]fluoro-3,6-dioxatetracosane ([18F]StP2)-labeled liposomes. Our results indicate that even a 1-mm diameter brain tumor could be imaged by PET, thus demonstrating the usefulness of these liposomes for PET imaging of brain cancer.

2. Materials and methods

2.1. Preparation of liposomes

All lipids were the products of Nippon Fine Chemical, Co. Ltd. (Takasago, Hyogo, Japan). Distearoylphosphatidylcholine (DSPC) and cholesterol along with DSPE-PEG or DSPE-PEG-APRPG (10:5:1 as a molar ratio) were dissolved in chloroform/*t*-butanol to formulate PEG-modified liposomes (PEG-liposomes) or APRPG–PEG-modified liposomes (APRPG-liposomes), respectively. For fluorescence labeling of liposomes, 1,1'-dioctadecyl-3,3,3',3'-tetramethyl-indocarbocyanine perchlorate (DiI, Molecular Probes Inc., Eugene, OR, USA) was added to the initial chloroform/*t*-butanol solution at a concentration of 1 mol% of DSPC. After the lipids had been dried under reduced pressure and stored *in vacuo* for at least 1 h, liposomes were prepared by hydration of the thin lipid film with 0.3 M glucose solution and frozen and thawed for 3 cycles by using liquid nitrogen. Then, the liposomes were sized by extruding them thrice through a polycarbonate membrane filter with 100-nm pores (Nuclepore track-Etch Membrane, Lipex). Particle size and ζ-potential of PEG-liposomes and APRPG-liposomes were measured by use of a Zetasizer Nano ZS (MALVERN, Worcestershire UK, USA) and found to be 113 nm and −2.0 mV, respectively, for PEG-liposomes and 107 nm and −3.3 mV, respectively, for the APRPG-liposomes.

2.2. Preparation of brain cancer-bearing model rats

The glioma-bearing rat model was prepared by a modification of the procedure described previously (Takeda et al., 2003). Nine-week-old Fischer 344 male rats (Japan SLC, Hamamatsu, Japan) were cared for according to the Animal Facility Guidelines of the University of Shizuoka. For the implantation of tumor cells, the rats were anesthetized with chloral hydrate (40 mg/kg) in saline and individually placed in a stereotaxic apparatus. C6 glioma cells were maintained in Dulbecco's modified Eagle medium (DMEM, Wako Fine Chemical Co. Ltd., Osaka, Japan) supplemented with 10% heat-inactivated fetal bovine serum (Japan Bioserum Co. Ltd., Japan), penicillin G (100 U/mL) and streptomycin (100 μg/mL) at 37 °C in 5% CO2 atmosphere. After harvesting of these cells, the cells were suspended in DMEM containing 1% gelatin (2 × 10⁷ cells/mL). Ten microliters of the cell suspension or vehicle (DMEM containing 1% gelatin) was injected at a rate of 0.7 μL/min into the left midbrain of each rat (4.3 mm posterior to bregma, 3.9 mm lateral to the midline suture, and 7.0 mm in depth) with an infusion pump (11 Plus, Harvard Apparatus, USA).

2.3. Intratumoral localization of DiI-labeled liposomes

C6 glioma cells (2.0 × 10⁵ cells/rat) were inoculated as described above. DiI-labeled liposomes were administered via a tail vein of the rat at 11 days after tumor implantation. One hour or 24 h after the injection of liposomes (0.5 mL/rat, 5 μmol as DSPC), the rats were anesthetized with chloral hydrate, perfused with *ca.* 200 mL saline and with *ca.* 100 mL 20% formaldehyde for the fixation. The brain was removed and sliced at a 2-mm thickness with a cryostat microtome (HM 505E, Microm, Walldorf, Germany). The slices were then incubated twice in PBS for 4 h each time at 4 °C, and then overnight in 30% sucrose solution at 4 °C. After removal of water, the slices were embedded in optimal cutting temperature compound (Sakura Finetech, Co. Ltd., Tokyo, Japan) and frozen at −80 °C. Brain sections (10 μm) were prepared with a cryostat microtome, and mounted on MAS-coated slides (Matsunami Glass Ind., Ltd., Japan) for observation with a fluorescence microscope (IMT-2, Olympus, Japan). Then, the slices were stained with hematoxylin and eosin (HE) and observed under the microscope.

2.4. Ex vivo imaging of the distribution of DiI-labeled liposomes

DiI-labeled liposomes (0.5 mL/rat, 5 μmol as DSPC) were administered via a tail vein of a rat at 9 days after the implantation of C6 glioma cells. One hour after the injection, the rats were sacrificed; and brain slices (2-mm thickness) were then prepared with a cryostat microtome without perfusion and fixation. Fluorescent images of those slices were obtained with a fluorescence imaging system (IVIS Lumina, Xenogen).

2.5. Preparation of positron emitter-labeled liposomes

Preparation of 1-[18F]fluoro-3,6-dioxatetracosane (StP2) and liposome labeling by the SophT method were performed as described previously (Urakami et al., 2007). About 100 MBq of [18F]StP2 in ethanol solution was transferred to a glass test tube, and the solvent was removed completely at 90 °C with a helium gas flow. Liposomal solution (1 mL, 10 μmol as DSPC) was added to the vial having a thin film of 18F-radiolabeled compound and incubated at 65 °C for 15 min with 5-s mixing by a vortex stirrer every 3 min. After the incubation, the liposomal solution was washed with PBS by centrifugation at 100,000 × *g* for 15 min (Beckman, Fullerton, CA, USA), and the pellet was resuspended and diluted in PBS to make a 22 MBq/mL solution. Radioactivity was measured with a curie meter (IGC-3, Aloka, Japan).

Rats anesthetized with chloral hydrate at 11 days after the implantation of C6 glioma cells were placed on an animal CT (Clairvivo CT, Shimadzu, Japan) to obtain CT images. Then, [^{18}F]SteP2-labeled liposomes (10 MBq/rat) were administered via a tail vein. PET scans were started immediately after the injection and continued for 60 min by use of an animal PET apparatus (Clairvivo PET, Shimadzu, Japan).

FDG-PET was similarly performed. [^{18}F]FDG (10 MBq/rat) was injected into the rats after having obtained the CT images.

2.6. PET analysis and autoradiography

Before PET analysis, rats anesthetized with chloral hydrate at 11 days after the implantation of C6 glioma cells were placed on the animal CT to obtain CT images. Then, [^{18}F]SteP2-labeled liposomes (10 MBq/rat) were administered via a tail vein. Then the PET scan was started immediately after the injection and continued for 60 min. FDG-PET was similarly performed. [^{18}F]FDG (10 MBq/rat) was injected into the rats after having obtained the CT images.

After the PET scan, the rats were sacrificed; and the brain was then excised. Thereafter, 2-mm slices were prepared and set on an imaging plate. Autoradiograms were obtained by using a bioimaging analyzer system (BAS2000, Fuji Film, Japan).

2.7. Biodistribution of liposomes

Glioma-bearing rats were injected with [^{18}F]SteP2-labeled PEG-liposomes (10 MBq/rat) via a tail vein. At day 1 h after the injection, the rats were sacrificed, and blood and organs (heart, lung, liver, spleen kidney normal part of brain, brain tumor) were removed. The radioactivity of blood and each organ was measured by using an auto gamma counter (1480 Wizard 3, Perkin Elmer, USA).

2.8. Statistical analysis

Differences between groups were evaluated by analysis of variance (ANOVA) with the Tukey *post hoc* test.

3. Results

3.1. Intratumoral distribution of fluorescence-labeled PEG- and APRPG-liposomes

At first, we confirmed that the angiogenic vessels formed by experimental glioma in the rat brain were leaky enough to allow permeation by nanomedicines such as liposomes. As shown in Fig. 1B and E, the DiI fluorescence of DiI-labeled PEG-liposomes and APRPG-liposomes, respectively, was observed in the glioma at 1 h after intravenous injection of the liposomes. Since DiI fluorescence was not observed in the normal brain tissues near the tumor, we concluded that the liposomes had accumulated in the tumor through angiogenic vessels. The fluorescence intensity was increased at 24 h after the injection (Fig. 1C and F). Interestingly, the DiI fluorescence of the PEG-liposomes accumulated widely in the tumor, although that of APRPG-liposomes accumulated intensely in rather specific areas, suggesting that these liposomes had accumulated in the angiogenic vessels. These patterns of liposomal fluorescence are consistent with our previous data obtained by use of tumor-bearing mice that had been implanted subcutaneously with C26 NL-17 colon carcinoma (Maeda et al., 2006).

To understand the structure of the brain vasculature, we examined normal and glioma-implanted brain specimens after HE-staining. As shown in Fig. 2, capillaries in the normal brain tissue were covered with astrocytes (Fig. 2A); whereas capillaries in the brain tumor tissues were surrounded directly by glioma cells (Fig. 2B). These results support the idea that the blood–brain barrier (BBB) is immature in angiogenic vessels of brain tumors. The possible architecture based on our observation and the literature (Standring, 2005) is shown in Fig. 2C and D.
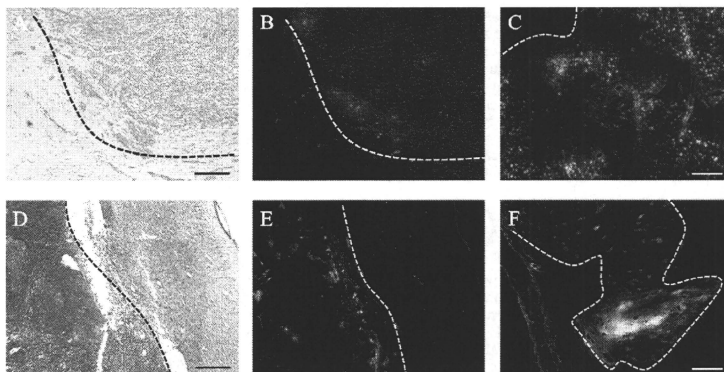

Fig. 1. Intratumoral distribution of fluorescence-labeled liposomes in brain tumor after intravenous injection. Rats were intravenously injected with DiI-labeled PEG-liposomes (A–C) or APRPG-liposomes (D–F) at day 11 after implantation of C6 glioma cells into the left midbrain. At 1 h (A, B, D, and E) or 24 h (C and F) after the injection, the brain tumors were dissected; and 10-μm frozen sections were prepared as described in Section 2. Then, liposomal distribution in the brain was observed under a fluorescence microscope (B, C, E, and F). Red fluorescence shows the liposomal localization. A and D show the images stained with hematoxylin and eosin, corresponding to the fluorescent images of "B" and "E", respectively. The dotted lines show the borders between normal and tumor tissue. Deep purple regions in "A" and "D" indicate the tumor tissues. The scale bar represents 100 μm.
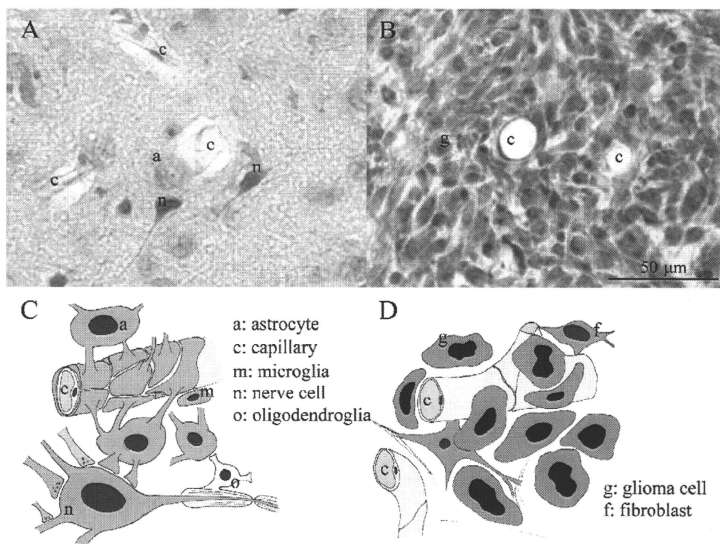
Fig. 2. Structure around blood capillaries in normal brain and brain tumor tissues. A rat brain tumor model was prepared by the implantation of C6 glioma cells into the left midbrain. The brain was dissected, and 10-μm sections of normal right brain (A) and tumor-implanted left brain (B) were stained with hematoxylin and eosin. Schematic interpretation of the histology around blood capillaries in normal brain (C) and brain tumor tissues (D) are shown.

3.2. Ex vivo study on the accumulation of fluorescence-labeled liposomes in brain tumor

Although microscopic study provided data on the intratumoral distribution of the liposomes, the liposomal distribution in the whole brain could not be understood. Therefore, we next examined the distribution of DiI-labeled liposomes in the glioma-bearing brain by use of whole-brain slices. As a result, both PEG-liposomes and APRPG-liposomes accumulated in the brain tumor 1 h after the injection via a tail vein (Fig. 3B and D, respectively). No specific accumulation could be observed in the sham-operated brain after the injection of the DiI-labeled PEG-liposomes (Fig. 3E and F). The fluorescence intensity of the tumor region was 4.0-fold and 3.1-fold higher than that of the contralateral regions after the injection of DiI-labeled PEG-liposomes and DiI-labeled APRPG-liposomes, respectively.

3.3. Brain tumor imaging with positron-emitter-labeled liposomes by PET

Finally, PEG-liposomes and APRPG-liposomes were labeled with the positron emitter [^{18}F]SteP2, by the SophT method, and injected into the glioma-bearing mice. As shown in Fig. 4, the positron emitter accumulated in the tumor region and imaged the tumor after injection in PEG-liposomes (Fig. 4, top panel) or APRPG-liposomes (Fig. 4, middle panel). Interestingly, the other regions of the brain showed a low background. On the contrary, [^{18}F]FDG imaged the whole brain, although the accumulation was higher in the tumor region (Fig. 4, bottom panel). BAS images (autoradiograms) shown in right panel confirmed the region of tumor. The tumor sizes of preparations varied to some extent in the present experiment, and

the smallest tumor was revealed to be only about 1 mm in diameter. Interestingly, this small tumor was imaged by PET but was hardly detectable by CT when [^{18}F]SteP2-labeled APRPG-liposomes had been injected (Fig. 5).

The biodistribution of ^{18}F at 1 h after the injection of [^{18}F]SteP2-labeled PEG-liposomes or [^{18}F]FDG is shown in Fig. 6. The liposome-bearing label was maintained in the bloodstream and highly accumulated in the spleen. This result is consistent with our previous study (Maeda et al., 2004). In the brain, ^{18}F in the liposomes or as FDG significantly accumulated more in the tumor than in the normal tissues. In contrast to the distribution of ^{18}F after injection of liposomes bearing it, ^{18}F as FDG was cleared from the bloodstream quite fast and accumulated in the heart and normal region of brain.

4. Discussion

Since the usefulness of FDG-PET for the detection of brain tumors is controversial (Takeda et al., 2003; Chen, 2007), other PET imaging agents have been developed. In the present study, we aimed at imaging brain tumors not by the synthesis of molecules specifically taken up by tumor cells, but by use of DDS technology. Nanocarriers such as liposomes are well known to accumulate in solid tumors, especially in hypervascular tumors, due to the EPR effect (Maeda et al., 2000, 2009). In fact, liposomal radionuclides show effective tumor imaging (Oku et al., 1996; Geng et al., 2004; Elbayoumi and Torchilin, 2006). Moreover, liposome-based radionuclide delivery is not only useful for cancer imaging but also for cancer therapy when the carriers entrapping radiopharmaceuticals or other anticancer agents are used (Kostarelos and
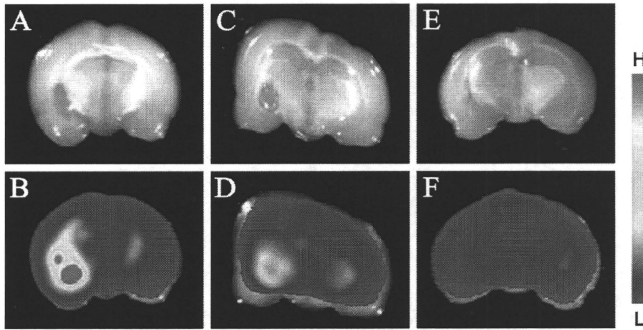
Fig. 3. Ex vivo imaging of liposomal distribution in rat brain bearing glioma. Rats were intravenously injected with Dil-labeled PEG-liposomes (A, B, E, and F) or APRPG-liposomes (C and D) at day 9 after implantation of C6 glioma cells (A–D) or medium alone (E and F) into the left midbrain. At 1 h after the injection, the brains were sliced into 2-mm sections, and the distribution of liposomes labeled with Dil was scanned with a fluorescence imaging system, IVIS (B, D, and F). Photos are also shown (A, C, and E). Two separate experiments gave similar results.

Emfietzoglou, 2000; Syme et al., 2003; Hamoudeh et al., 2008). Another advantage of carrier-based imaging is the active targeting by modifying carriers with some specific probes. We previously modified liposomes with angiogenic vessel-specific peptides and observed the efficient delivery of targeting liposomes to cancer by PET (Kondo et al., 2004; Maeda et al., 2006). Therefore, cancer imaging with DDS technology has various advantages including cancer treatment.
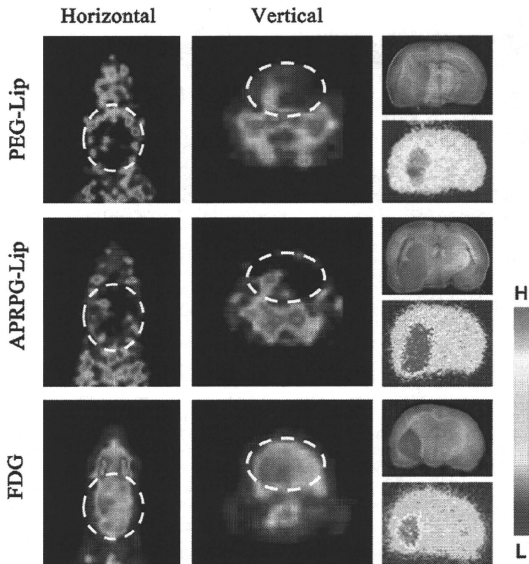

Fig. 4. PET imaging of brain tumor with [18F]SteP2-liposomes and [18F]-FDG. Rats were intravenously injected with 10 MBq of [18F]SteP2-labeled PEG-liposomes (top panel), [18F]SteP2-labeled APRPG-liposomes (middle panel) or [18F]FDG (bottom panel) at day 11 after implantation of C6 glioma cells into the left midbrain. The biodistribution pattern of samples was determined by taking 1 frame/min for 1 h with the Clairvivo PET, and averaged data from 40 to 60 min are shown. Horizontal (left panel) and vertical (center panel) images are shown. After PET imaging, the brains were sliced into 2-mm sections, and the autoradiograms (right lower panels) were obtained with a bioimaging analyzer BAS 2000, and the pictures were taken (right upper panels). The ovals formed by the white dotted line show the estimated brain position.
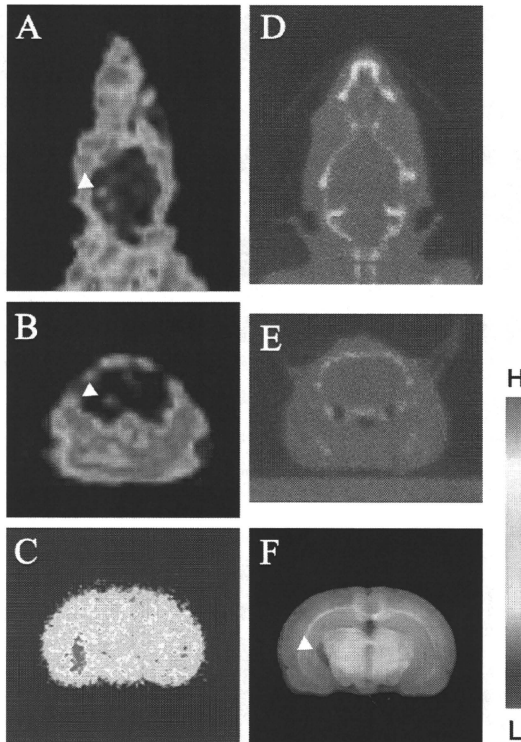
Fig. 5. PET imaging of small brain tumor with [^{18}F]SteP2-liposomes. PET imaging was performed as described in the legend of Fig. 4. Even the smallest tumor, 1-mm diameter, seen among the prepared model rats was imaged by PET. PET images (A and B) and CT images (D and E) of a rat brain are shown. Horizontal (A and D) and vertical (B and E) images are shown. (C) BAS image of a rat brain slice. (F) Photo of the brain slice. Arrowheads indicate the tumor.

It is well known that glioblastoma, the most prevalent brain cancer, is a hypervascular tumor due to angiogenesis (Verhoeff et al., 2009; Brastianos and Batchelor, 2009); and thus nanocarriers such as liposomes would be expected to accumulate in the brain cancer, since the permeability of tumor angiogenic vessels was higher than that of normal blood vessels. Moreover, brain blood vessels especially protect from the penetration of some molecules due to the BBB. Therefore, liposomes or other nanocarriers would be specifically accumulated into brain tumor region after circulating bloodstream, and be useful for brain cancer imaging. For labeling nanocarriers quite conveniently with PET probes, we previously synthesized a novel ^{18}F-labeled amphiphilic compound known as 1-[^{18}F]fluoro-3,6-dioxatetracosane (Urakami et al., 2007). There are several methods for labeling liposomes, although radionuclides need to be incorporated during formulation of the liposomes in most of those methods. For example, to label liposomes with [^{18}F]FDG, [^{18}F]FDG was incorporated into liposomal aqueous phase during hydration step of liposomal lipids. In addition, the encapsulation efficiency of [^{18}F]FDG into the liposomes was very low. The

advantage of the "solid-phase transition" (SophT) method is that it is applicable to preformed liposomes with quite high labeling efficiency. Moreover, [^{18}F]SteP2 in DSPC-based liposomes is stable in the presence of serum (Urakami et al., 2007). This universal method of liposomal modification can be used for various kinds of liposomes and lipidic nanoparticles and bring the enhanced detection of a target tissue.

Aim of the present study is to demonstrate the application of positron-labeled liposomes for brain tumor imaging by PET. We firstly examined the intratumoral distribution of fluorescence-labeled PEG- and APRPG-liposomes by fluorescence microscopy, and observed the accumulation of both DiI-labeled PEG-liposomes and APRPG-liposomes in the brain tumor region at 1 h after intravenous injection of the liposomes, although the intratumoral distribution of each liposome was different. We previously demonstrated that PEG-liposomes were accumulated around neovessels and fluorescence of DiI-labeled-APRPG-liposomes was colocalized with CD31 stain in colon 26 NL-17 solid tumor (Maeda et al., 2006). Therefore, the differential accumulation
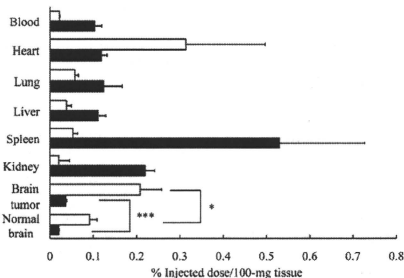
Fig. 6. Biodistribution of ^{18}F after injection of [^{18}F]SteP2-labeled PEG-liposomes or [^{18}F]-FDG. Injection of [^{18}F]SteP2-labeled liposomes and [^{18}F]-FDG was performed as described in the legend of Fig. 4. At 1 h after the injection, blood was collected; and the selected organs were then excised for the determination of the radioactivity. Data are presented as the mean distribution of ^{18}F after injection of [^{18}F]SteP2-labeled PEG-liposomes (closed bars, $n = 3$) or [^{18}F]FDG (open bars, $n = 4$). Significant differences between normal and tumor tissues are shown: *$p < 0.05$, ***$p < 0.001$.

of PEG-liposomes and APRPG-liposomes observed in the tumor region, might be caused by the APRPG-modification of the latter liposomes.

In the present study HE-staining of normal brain tissue indicated that the capillaries were wrapped with astrocytes, whose arrangement may strengthen the BBB function (Standring, 2005). In contrast, astrocytes and nerve cells were not observed in the brain tumor tissues, and the capillaries directly faced the surrounding glioma cells: This might support the extravasation of PEG-liposomes into the tumor tissues. On the other hand, APRPG-liposomes might specifically accumulate in angiogenic vessels in brain tumor tissue. Ex vivo imaging of DiI with the in vivo fluorescence imaging system indicated the accumulation of both PEG-liposomes and APRPG-liposomes in the brain tumor was 3–4 fold higher than that in the surrounding normal brain tissue.

Our PET study indicated the accumulation of ^{18}F-labeled liposomes and imaging of glioma in the tumor-bearing rat brain. The tumor images obtained with liposomes were clearer than those obtained with FDG-PET. In the case of [^{18}F]FDG imaging, the background level represented by imaging of normal brain region was high, since persistent demand for glucose to normal brain cells (Fig. 5). In contrast, brain tumor was specifically imaged by using [^{18}F]-labeled PEG- or APRPG-liposomes with quite low background. Additionally, these liposomes also can be used for the brain cancer therapy.

The efficiency for tumor imaging by both [^{18}F]SteP2-labeled PEG-liposomes and APRPG-liposomes was similar, although the intratumoral distribution was different between PEG-liposomes and APRPG-liposomes. These data are consistent with our previous results showing that the accumulation of PEG-liposomes and APRPG-liposomes in solid tumors was not much different (Maeda et al., 2004). Therefore, we conclude that [^{18}F]-labeled liposomes having either passive or active targeting characteristics are useful for brain tumor imaging; However, active targeting liposomes to tumor angiogenic endothelium would be more potent when these are used for both imaging and therapy. In the present study, it should be also noted that a tumor with a diameter of only 1 mm could be successfully imaged by using [^{18}F]SteP2-labeled liposomes.

5. Conclusions

In the present study, brain tumor imaging by a DDS nanocarrier, i.e., liposomes, was explored. Liposomes were ^{18}F-labeled by the Sopht method and injected intravenously into rats bearing a glioma-type brain tumor. Liposomes failed to accumulate in the normal surrounding brain tissue due to BBB protection and a brain tumor was specifically imaged with the liposomes via the different structure of brain tumor vessels. Since radiopharmaceutics or anticancer agents can be incorporated into DDS nanocarriers, these nanocarriers including liposomes should be useful for diagnosis and therapy of brain cancer.

References

Asai, T., Shimizu, K., Kondo, M., Kuromi, K., Watanabe, K., Ogino, K., Taki, T., Shuto, S., Matsuda, A., Oku, N., 2002. Anti-neovascular therapy by liposomal DPP-CNDAC targeted to angiogenic vessels. FEBS Lett. 520, 167–170.
Brastianos, P.K., Batchelor, T.T., 2009. VEGF inhibitors in brain tumors. Clin. Adv. Hematol. Oncol. 768, 753–760.
Chen, W., 2007. Clinical applications of PET in brain tumors. J. Nucl. Med. 48, 1468–1481.
Elbayoumi, T.A., Torchilin, V.P., 2006. Enhanced accumulation of long-circulating liposomes modified with the nucleosome-specific monoclonal antibody 2C5 in various tumours in mice: gamma-imaging studies. Eur. J. Nucl. Med. Mol. Imaging 33, 1196–1205.
Floeth, F.W., Pauleit, D., Sabel, M., Stoffels, G., Reifenberger, G., Riemenschneider, M.J., Jansen, P., Coenen, H.H., Steiger, H.J., Langen, K.J., 2007. Prognostic value of O-(2-[18]fluoroethyl)-L-tyrosine PET and MRI in low-grade glioma. J. Nucl. Med. 48, 519–527.
Gabizon, A.A., 2001. Pegylated liposomal doxorubicin: metamorphosis of an old drug into a new form of chemotherapy. Cancer Invest. 19, 424–436.
Geng, L., Osusky, K., Konjeti, S., Fu, A., Hallahan, D., 2004. Radiation-guided drug delivery to tumor blood vessels results in improved tumor growth delay. J. Control. Release 99, 369–381.
Hamoudeh, M., Kamleh, M.A., Diab, R., Fessi, H., 2008. Radionuclide delivery systems for nuclear imaging and radiotherapy of cancer. Adv. Drug Deliv. Rev. 60, 1329–1346.
Hatakeyama, T., Kawai, N., Nishiyama, Y., Yamamto, Y., Sasakawa, Y., Ichikawa, T., Tamiya, T., 2008. ^{11}C-methionine (MET) and ^{18}F-fluorothymidine (FLT) PET in patients with newly diagnosed glioma. Eur. J. Nucl. Med. Mol. Imaging 35, 2009–2017.
Heiss, P., Mayer, S., Herz, M., Wester, H.J., Schwaiger, M., Senekowitsch-Schmidtke, R., 1999. Investigation of transport mechanism and uptake kinetics of O-(2-[18]fluoroethyl)-L-tyrosine in vitro and in vivo. J. Nucl. Med. 40, 1367–1673.
Ishiwata, K., Kawamura, K., Wang, W.F., Furumoto, S., Kubota, K., Pascali, C., Bogni, A., Iwata, R., 2004. Evaluation of O-[^{11}C]methyl-L-tyrosine and O-[^{18}F]fluoromethyl-L-tyrosine as tumor imaging tracers by PET. Nucl. Med. Biol. 31, 191–198.
Jager, P.L., Vaalburg, W., Pruim, J., de Vries, E.G., Langen, K.J., Piers, D.A., 2001. Radio-labeled amino acids: basic aspects and clinical applications in oncology. J. Nucl. Med. 42, 432–445.
Kato, T., Shinoda, J., Nakayama, N., Miwa, K., Okumura, A., Yano, H., Yoshimura, S., Maruyama, T., Muragaki, Y., Iwama, T., 2008. Metabolic assessment of gliomas using ^{11}C-methionine, [^{18}F] fluorodeoxyglucose, and ^{11}C-choline positron-emission tomography. AJNR Am. J. Neuroradiol. 29, 1176–1182.
Kondo, M., Asai, T., Katanasaka, Y., Sadzuka, Y., Tsukada, H., Ogino, K., Taki, T., Baba, K., Oku, N., 2004. Anti-neovascular therapy by liposomal drug targeted to membrane type-1 matrix metalloproteinase. Int. J. Cancer 108, 301–306.
Kostarelos, K., Emfietzoglou, D., 2000. Tissue dosimetry of liposome–radionuclide complexes for internal radiotherapy: toward liposome-targeted therapeutic radiopharmaceuticals. Anticancer Res. 20, 3339–3345.
Langen, K.J., Hamacher, K., Weckesser, M., Floeth, F., Stoffels, G., Baur, D., Coenen, H.H., Pauleit, D., 2006. O-(2-[^{18}F]fluoroethyl)-L-tyrosine: uptake mechanisms and clinical applications. Nucl. Med. Biol. 33, 287–294.
Maeda, H., Wu, J., Saw, T., Matsumura, Y., Hori, K., 2000. Tumor vascular permeability and the EPR effect in macromolecular therapeutics: a review. J. Control. Release 65, 271–284.
Maeda, H., Bharate, G.Y., Daruwalla, J., 2009. Polymeric drugs for efficient tumor-targeted drug delivery based on EPR-effect. Eur. J. Pharm. Biopharm. 71, 409–419.
Maeda, N., Takeuchi, Y., Takada, M., Sadzuka, Y., Namba, Y., Oku, N., 2004. Anti-neovascular therapy by use of tumor neovasculature-targeted long-circulating liposome. J. Control. Release 100, 41–52.
Maeda, N., Miyazawa, S., Shimizu, K., Asai, T., Yonezawa, S., Kitazawa, S., Namba, Y., Tsukada, H., Oku, N., 2006. Enhancement of anticancer activity in antineovascular therapy is based on the intratumoral distribution of the active targeting carrier for anticancer drugs. Biol. Pharm. Bull. 29, 1936–1940.
Mehrkens, J.H., Pöpperl, G., Rachinger, W., Herms, J., Seelos, K., Tatsch, K., Tonn, J.C., Kreth, F.W., 2008. The positive predictive value of O-(2-[^{18}F]fluoroethyl)-

L-tyrosine (FET) PET in the diagnosis of a glioma recurrence after multimodal treatment. J. Neurooncol. 88, 27–35.

Nakamoto, Y., Togashi, K., Kaneta, T., Fukuda, H., Nakajima, K., Kitajima, K., Murakami, K., Fujii, H., Satake, M., Tateishi, U., Kubota, K., Senda, M., 2009. Clinical value of whole-body FDG-PET for recurrent gastric cancer: a multicenter study. Jpn. J. Clin. Oncol. 39, 297–302.

Nojiri, T., Nariai, T., Aoyagi, M., Senda, M., Ishii, K., Ishiwata, K., Ohno, K., 2009. Contributions of biological tumor parameters to the incorporation rate of L-[methyl-^{11}C] methionine into astrocytomas and oligodendrogliomas. J. Neurooncol. 93, 233–241.

Oku, N., Tokudome, Y., Tsukada, H., Kosugi, T., Namba, Y., Okada, S., 1996. In vivo trafficking of long-circulating liposomes in tumour-bearing mice determined by positron emission tomography. Biopharm. Drug Dispos. 17, 435–441.

Oku, N., Asai, T., Watanabe, K., Kuromi, K., Nagatsuka, M., Kurohane, K., Kikkawa, H., Ogino, K., Tanaka, M., Ishikawa, D., Tsukada, H., Momose, M., Nakayama, J., Taki, T., 2002. Anti-neovascular therapy using novel peptides homing to angiogenic vessels. Oncogene 21, 2662–2669.

Pauleit, D., Stoffels, G., Bachofner, A., Floeth, F.W., Sabel, M., Herzog, H., Tellmann, L., Jansen, P., Reifenberger, G., Hamacher, K., Coenen, H.H., Langen, K.J., 2009. Comparison of ^{18}F-FET and ^{18}F-FDG PET in brain tumors. Nucl. Med. Biol. 36, 779–787.

Sakakibara, T., Chen, F.A., Kida, H., Kunieda, K., Cuenca, R.E., Martin, F.J., Bankert, R.B., 1996. Doxorubicin encapsulated in sterically stabilized liposomes is superior to free drug or drug-containing conventional liposomes at suppressing growth and metastases of human lung tumor xenografts. Cancer Res. 56, 3743–3746.

Scott, A.M., Gunawardana, D.H., Bartholomeusz, D., Ramshaw, J.E., Lin, P., 2008. PET changes management and improves prognostic stratification in patients with head and neck cancer: results of a multicenter prospective study. J. Nucl. Med. 49, 1593–1600.

Standring, S., 2005. GRAY'S Anatomy, 39th ed. Elsevier, Edinburgh, pp. 51–52.

Syme, A.M., McQuarrie, S.A., Middleton, J.W., Fallone, B.G., 2003. Dosimetric model for intraperitoneal targeted liposomal radioimmunotherapy of ovarian cancer micrometastases. Phys. Med. Biol. 48, 1305–1320.

Takeda, A., Tamano, H., Oku, N., 2003. Alteration of zinc concentrations in the brain implanted with C6 glioma. Brain Res. 965, 170–173.

Tang, G., Wang, M., Tang, X., Luo, L., Gan, M., 2003. Synthesis and evaluation of O-(3-[18F]fluoropropyl)-L-tyrosine as an oncologic PET tracer. Nucl. Med. Biol. 30, 733–739.

Tian, M., Zhang, H., Oriuchi, N., Higuchi, T., Endo, K., 2004. Comparison of ^{11}C-choline PET and FDG PET for the differential diagnosis of malignant tumors. Eur. J. Nucl. Med. Mol. Imaging 31, 1064–1172.

Ullrich, R.T., Kracht, L., Brunn, A., Herholz, K., Frommolt, P., Miletic, H., Deckert, M., Heiss, W.D., Jacobs, A.H., 2009. Methyl-L-^{11}C-methionine PET as a diagnostic marker for malignant progression in patients with glioma. J. Nucl. Med. 50, 1962–1968.

Urakami, T., Akai, S., Katayama, Y., Harada, N., Tsukada, H., Oku, N., 2007. Novel amphiphilic probes for [18F]-radiolabeling preformed liposomes and determination of liposomal trafficking by positron emission tomography. J. Med. Chem. 50, 6454–6457.

Urakami, T., Sakai, K., Asai, T., Fukumoto, D., Tsukada, H., Oku, N., 2009. Evaluation of O-[18F]fluoromethyl-D-tyrosine as a radiotracer for tumor imaging with positron emission tomography. Nucl. Med. Biol. 36, 295–303.

Verhoeff, J.J., Stalpers, L.J., Claes, A., Hovinga, K.E., Musters, G.D., Vandertop, W.P., Richel, D.J., Leenders, W.P., van Furth, W.R., 2009. Tumour control by whole brain irradiation of anti-VEGF-treated mice bearing intracerebral glioma. Eur. J. Cancer 45, 3074–3080.

Wen, P.Y., Kesari, S., 2008. Malignant gliomas in adults. N. Engl. J. Med. 359, 492–507.

Yamamoto, Y., Nishiyama, Y., Kimura, N., Kameyama, R., Kawai, N., Hatakeyama, T., Kaji, M., Ohkawa, M., 2008. ^{11}C-acetate PET in the evaluation of brain glioma: comparison with ^{11}C-methionine and ^{18}F-FDG-PET. Mol. Imaging Biol. 10, 281–287.

Cancer antineovascular therapy with liposome drug delivery systems targeted to BiP/GRP78

Yasufumi Katanasaka[1,2,3], Takayuki Ishii[1,2], Tomohiro Asai[1,2], Hirotaka Naitou[2,4], Noriyuki Maeda[5], Fumiaki Koizumi[3], Shinichi Miyagawa[6], Norio Ohashi[2,7] and Naoto Oku[1,2]

[1] Department of Medical Biochemistry, Graduate School of Pharmaceutical Sciences, University of Shizuoka, Suruga-ku, Shizuoka, Japan
[2] Global COE Program, University of Shizuoka, Suruga-ku, Shizuoka, Japan
[3] Shien-Lab, National Cancer Center Hospital, Chuo-ku, Tokyo, Japan
[4] Laboratory of Environmental Microbiology, Institute for Environmental Sciences, University of Shizuoka, Shizuoka, Japan
[5] Nippon Fine Chemical, Ltd., Takasago, Hyogo, Japan
[6] Department of Surgery, Shinshu University School of Medicine, Matsumoto, Nagano, Japan
[7] Laboratory of Microbiology, Graduate School of Nutritional and Environmental Sciences, University of Shizuoka, Shizuoka, Japan

Angiogenesis is crucial for tumor growth and hematogenous metastasis. Specifically expressed and functional protein molecules in angiogenic endothelial cells, especially on the plasma membrane, may be molecular targets for antiangiogenic drugs and drug delivery systems (DDS) in cancer therapy. To discover such target molecules, we performed subcellular proteome analysis of human umbilical vein endothelial cells (HUVECs) treated with or without vascular endothelial growth factor (VEGF) using 2-dimensional difference in-gel electrophoresis (2D-DIGE) and matrix-assisted laser desorption/ionization tandem time-of-flight mass spectrometry (MALDI-TOF/TOF-MS). Among the identified proteins, BiP/GRP78, a molecular chaperone, was highly expressed in the membrane/organelle fraction of HUVECs after VEGF treatment. The involvement of BiP in VEGF-induced angiogenesis was examined by RNA interference. BiP knockdown significantly suppressed VEGF-induced endothelial cell proliferation and VEGF-induced phosphorylation of extracellular-regulated kinase 1/2, phospholipase C-γ, and VEGF receptor-2 in HUVECs. Cell surface biotinylation analysis revealed that the cell surface expression of BiP was elevated in VEGF-activated HUVECs. Aiming to apply BiP to a target molecule in liposomal DDS, we developed liposomes modified with the WIFPWIQL peptide, which has been shown to bind to BiP, and investigated its potential for cancer therapy. The WIFPWIQL-modified liposomes (WIFPWIQL liposomes) were significantly taken up by VEGF-activated HUVECs as compared to peptide-unmodified liposomes. WIFPWIQL liposomes appeared to accumulate in tumor endothelial cells *in vivo*. WIFPWIQL liposomes containing doxorubicin significantly suppressed tumor growth and prolonged the survival of colon26 NL-17 carcinoma cell-bearing mice. In summary, BiP may regulate VEGF-induced endothelial cell proliferation through VEGFR-2-mediated signaling and be an effective target molecule for cancer antineovascular therapy.

Angiogenesis, the process of sprouting new blood vessels from preexisting vessels, is critical for tumor growth and blood-borne metastasis.[1] The overall process of angiogenesis is regulated by the balance between proangiogenic and antiangiogenic factors secreted from several cell types in a tumor microenvironment, such as tumor cells, fibroblasts and macrophages.[2,3] Endothelial cells in tumors differentially express various protein molecules compared to those in normal tissues.[4] In intratumoral regions, under hypoxic conditions, tumor cells produce vascular endothelial growth factor

Cancer Therapy

(VEGF), a principal proangiogenic factor, through hypoxia-inducible factor 1-dependent transcription.[5] VEGF and its receptor (VEGFR) have been well studied in basic and clinical cancer research, and inhibitors of VEGF signal transduction have been developed as anticancer drugs.[6] The activation of VEGFRs initiates the proliferation, migration and invasion of endothelial cells. VEGF induces the phosphorylation of VEGFR tyrosine kinases, and thereby activates mitogen-activated protein kinase (MAPK) mediated by phospholipase C-γ (PLCγ) or the AKT/PKB signal cascade mediated by phosphatidylinositol-3 kinase (PI3K).[7]

Comparative proteome analysis is a powerful tool to find differentially expressed proteins[8,9]; and it is rendered more powerful by combining it with subcellular fractionation, whereby it can identify low-abundance proteins in cellular organelles by subtracting out common protein contaminants.[10,11] The proteins on the plasma membrane play a role in fundamental cellular processes, including ion and solute transports, signal transduction or cell adhesion. Since alterations in the expression of membrane proteins are often related to diseases, such proteins may become molecular targets for diagnostic and therapeutic approaches.[12–14] Comprehensive profiling of these proteins may also provide a better understanding of how a cell responds to a variety of intracellular and extracellular signals. Therefore, expression profiling of membrane proteins in specific cell types under defined conditions has become a central point of many molecular biology investigations.

Inhibition of angiogenesis has curative benefits such as inhibition of primary tumor growth as well as suppression of blood-borne metastasis.[15] Therapeutic vascular targeting has been categorized into antiangiogenic approaches, which aim to prevent the neovascularization processes in tumors, whereas vascular-disrupting approaches—using vascular disrupting agents—aim to damage the established tumor vasculature.[16] Antineovascular therapy is a strategy targeted against angiogenic neovasculature by using liposome drug delivery systems (DDS).[17–19] We and other groups have previously reported that tumor vasculature-targeted liposomes can deliver encapsulated agents to angiogenic endothelial cells and have demonstrated their therapeutic advantages.[20,21] Cell surface proteins specifically expressed in angiogenic endothelial cells are possible molecular targets for DDS because these cells are in direct contact with the blood stream, making it easy for drug carriers to recognize them after modifying these carriers with appropriate targeting tools such as antibodies, peptides or carbohydrates. However, it appears that there are few target molecules for tumor vasculature-targeted drug delivery, and the identification of novel target molecules would contribute to the development of DDS in cancer therapeutics.

Here, we describe subcellular proteome analysis of human umbilical vein endothelial cells (HUVECs) treated with or without VEGF to discover the target molecules expressed on the cellular membranes of angiogenic endothelial cells using 2-dimensional difference in-gel electrophoresis (2D-DIGE)

and matrix-assisted laser desorption/ionization tandem time-of-flight mass spectrometry (MALDI-TOF/TOF-MS); and then describe the functional analysis of BiP (immunoglobulin heavy chain-binding protein), which is also called glucose-regulated protein 78 kDa (GRP78) and is an identified protein in the proteomic analysis. Moreover, we developed BiP-targeted liposomes and evaluated the utility of BiP-targeted drug delivery in cancer antineovascular therapy.

Material and Methods

Cell culture

HUVECs (Cambrex Corporation, Walkersville, MD) were maintained in endothelial growth medium-2 (EGM-2, Cambrex Corporation) at 37°C under 5% CO_2 in a humidified chamber, as described previously.[17] HUVECs were used at passage 7 or less in all the experiments. Mouse colon26 NL-17 carcinoma cells (C26) and human prostate carcinoma DU145 cells were cultured in an appropriate medium supplemented with streptomycin (100 μg/mL), penicillin (100 units/mL) and 10% heat-inactivated fetal bovine serum (FBS) at 37°C in 5% CO_2.

Cellular protein fractionation

HUVECs were grown to subconfluence (80–90% confluence) in T-150 flasks, and the culture medium was replaced with 0.5% FBS-containing endothelial basal medium-2 (EBM-2, Cambrex Corporation). After serum starvation by overnight incubation, recombinant human VEGF$_{165}$ (rhVEGF, 20 ng/ml as final concentration; BD Biosciences, San Diego, CA) was added to the starved cells, which were then further incubated for 24 hr at 37°C. The cells were washed with ice-cold PBS (pH 7.4), and the proteins in the membrane/organelle were separately extracted using a Subcellular Proteome Extraction Kit (Calbiochem, San Diego, CA) according to the manufacturer's recommended protocol. The proteins in each fraction were precipitated using a Protein Precipitant Kit (Calbiochem) to concentrate the proteins and to remove interfering substances according to the manufacturer's recommended protocol. The precipitated proteins were then resolubilized in lysis buffer for 2D-DIGE (7 M urea, 2 M thiourea, 4% CHAPS, 30 mM Tris-HCl; pH 8.5), and the protein concentration was determined by the Bradford protein assay method (Bio-Rad Laboratories, Tokyo, Japan).

2D-DIGE

2D-DIGE was performed as previously described,[22] and reagents used for 2D-DIGE were purchased from GE Healthcare UK (Buckinghamshire, UK). An internal standard was prepared by pooling an equal amount of each protein from VEGF-stimulated and nonstimulated HUVECs. Then, 50 μg of protein from the internal standard, nontreated sample and VEGF-stimulated sample was fluorescence-labeled with 400 pmol of Cy2, Cy3 and Cy5, respectively, on ice for 30 min in the dark. The labeling reaction was quenched with 10 mM L-lysine. The fluorescently labeled samples were mixed and

adjusted to a final volume of 450 μL with rehydration buffer (7 M urea, 2 M thiourea, 2% CHAPS, 1% DTT and 0.002% bromophenol blue). The samples were applied to isoelectric focusing polyacrylamide gel electrophoresis (IEF) using IPG strips (pH 3–10, nonlinear, 24 cm) and IPGphor II. The IPG strips were rehydrated with CyDye-labeled samples at 20°C for 12 hr, and IEF was performed in Ipgphor at 20°C with a total of 80 kVh. The IPG strips were equilibrated for 15 min by shaking gently in an equilibration buffer (6 M urea, 30% glycerol, 2% SDS, 1.5 M Tris-HCl; pH 8.8) containing DTT (10 mg/mL) and then for 15 min in an equilibration buffer containing iodoacetoamide (25 mg/mL) instead of DTT. The equilibrated IPG strips were transferred onto 10% polyacrylamide gels and 2D electrophoresis was performed using the Ettan Dalt II system. The 2D-gel images were scanned at appropriate wavelengths for Cy2, Cy3 and Cy5 dyes with a Typhoon 9400^{TM} scanner; and the spot volumes were analyzed quantitatively using the biological variation analysis (BVA) mode of DyCyder software (version 5.0). Spots of interest were defined from average ratios of VEGF-stimulated over nonstimulated, which were above 1.5 or below −1.5-fold (0.67-fold) with significant difference (4 separate gels, Student's *t*-test, $p < 0.05$).[23]

Mass spectrometry and protein identification
For mass spectrometry analysis, 500 μg of the pooled proteins was applied to 2D electrophoresis and then stained with Deep Purple, according to the manufacturer's instructions. The gel was imaged with a Typhoon 9400 scanner. The matched spots of interest were picked with Ettan Spot Picker. In-gel digestion was performed as follows. The gel pieces picked were destained with 50 mM NH_4HCO_3 in 50% acetonitrile (ACN) and dehydrated with 100% ACN. The dried gel pieces were added to trypsin solution (25 ng/mL, Promega, Madison, WI) and incubated overnight at 37°C. The digested peptides were extracted with 1% trifluoroacetic acid (TFA) in 80% ACN and concentrated with a vacuum centrifuge. The peptide solutions were desalted and concentrated with Zip-Tip C18μ (Millipore, Bedford, MA). Then, the peptide solutions were mixed with α-cyano-4-hydroxycinnamic acid (Sigma, Tokyo, Japan) and applied onto a target plate (Bruker Daltonics, Bremen, Germany). The MS and MS/MS spectra were obtained using an Ultraflex mass spectrometer (Bruker Daltonics) in the reflector mode. The acquired spectra were analyzed using Flexanalysis software (version 2.2, Bruker Daltonics) in the default mode. The protein species were identified by peptide mass fingerprinting and/or combined search using Biotool software (version 2.2, Bruker Daltonics) and the Mascot search engine (version 2.0, Matrix Science, London, UK) against the NCBI database.

Western blot analysis
Western blotting was performed as described previously[24] with some modifications. The cells were washed with ice-cold PBS and lysed with 10 mM Tris-HCl (pH 7.4) containing

0.1% SDS, 2 mM phenylmethylsulfonyl fluoride (PMSF), 50 μg/mL aprotinin, 200 μM leupeptin and 100 μM pepstatin A. To examine the phosphorylation of VEGFR-2, PLCγ and ERK1/2, we stimulated starved HUVECs with rhVEGF for 5 or 10 min. The protein concentration was determined by using the BCA protein assay kit (Pierce, Tokyo, Japan). The protein samples were mixed with SDS-PAGE sample buffer (2% SDS, 10% glycerol, 6% 2-mercaptoethanol, 50 mM Tris-HCl; pH 6.8), and an equal amount of proteins in each sample was subjected to SDS-PAGE. The separated proteins were transferred to a PVDF membrane (Millipore) and blocked with 5% skim-milk in TBST (0.9% NaCl, 0.1% Tween20, 20 mM Tris-HCl; pH7.4). The primary antibodies used were anti-GRP78 (BiP) antibody (Santa Cruz Biotechnology, San Diego, CA), antiactin antibody (Sigma), anti-GAPDH antibody (Abcam, Cambridge, UK), antiphospho-ERK1/2 (Thr183/Tyr185), anti-ERK1/2 (Promega), antiphospho-PLCγ1 (Tyr783), anti-PLCγ1, antiphospho-VEGFR-2 (Tyr1175) and anti-VEGFR-2 (Cell Signaling Technology, Beverly, MA). Horseradish peroxidase (HRP)-conjugated antibodies were used as secondary antibodies. The PVDF membrane was developed with ECL reagent (GE Healthcare). The band density was measured with ImageJ software.

Cell-surface biotinylation
Extraction of cell-surface proteins was performed with a Cell Surface Biotinylation Kit (Pierce) according to the manufacturer's instructions. In brief, HUVECs were washed with ice-cold PBS, treated with NHS-SS-Biotin, and further incubated at 4°C for 30 min to conjugate the cell-surface proteins with NHS-SS-Biotin. After quenching the protein-NHS reaction, the cells were scraped and centrifuged at 500g for 3 min at 4°C. The cell pellets were then solubilized by sonication in the manufacturer's supplied lysis buffer and centrifuged at 10,000g for 3 min at 4°C. The protein samples in the supernatant were applied to a NeutrAvidin^{TM} column and the biotin-conjugated cell-surface proteins were eluted with 50 mM DTT-containing buffer (0.1% SDS, 62.5 mM Tris-HCl; pH 6.8).

RNA interference
RNA interference (RNAi) was performed with Dharma-FECT^{TM} reagent (GE Healthcare) according to the manufacturer's instructions. HUVECs were seeded at 2.0×10^5 cells (80–90% confluence) in an antibiotic-free EGM-2 medium and incubated overnight. The cells were transfected with 100 nM of small interfering RNA (siRNA, Hokkaido System Sciences, Hokkaido, Japan) using DharmaFECT^{TM} reagent. The sequences of siRNA for BiP (BiP siRNA) were 5′-GGU UAC CCA UGC AGU UGU UTT-3′ (sense) and 5′-AAC AAC UGC AUG GGU AAC CTT-3′ (antisense), as previously described.[25] The sequences of siRNA for green fluorescent protein (GFP siRNA used as nonsilencing control siRNA) have been described previously.[26] After incubation with these siRNAs for 48 hr at 37°C, the effects of each siRNA on

37

protein expression were determined by Western blot analysis and real-time PCR.

RNA isolation and real-time PCR

Total RNA was isolated using ISOGEN (Nippon Gene, Tokyo, Japan) and the resulting RNA was reverse transcribed. TaqMan real-time PCR assay was performed using TaqMan gene expression assays on a StepOnePlus (Applied Biosystems, Tokyo, Japan). The relative real-time PCR quantification was based on a comparative quantitation method. The endogenous reference gene was GAPDH. The specificity of the PCR reactions was confirmed by a single band of the predicted size after agarose gel electrophoresis (data not shown).

Cell proliferation assay

HUVECs were transfected with each siRNA as described above and incubated for 24 hr at 37°C. The transfected cells were harvested and reseeded at 2.0×10^4 cells per well on a 24-well plate in 0.5% FBS-containing EBM-2 medium with or without rhVEGF (20 ng/mL). The cells were further incubated for 24 or 48 hr, and the cell viability was determined at each time with TetraColor One™ (Seikagaku, Tokyo, Japan). The growth ratio was calculated by the absorbance (450 nm) at 24 hr/3 hr and 48 hr/3 hr. The absorbance at 3 hr was considered to reflect the cell number immediately after seeding the cells without cell proliferation.

Preparation of liposomes

Distearoyl phosphatidylcholine (DSPC), distearoyl phosphatidylglycerol (DSPG), cholesterol and distearoyl phosphatidylethanolamine-conjugated polyethyleneglycol 2000 (DSPE-PEG) or the DSPE-PEG conjugate of GWIFPWIQL-peptides, which are shown to bind to BiP/GRP78,[27] were dissolved in tert-butylalcohol (10:10:10:1 as a molar ratio). The lipid solutions were lyophilized, and the lyophilizates were hydrated with 0.3 M sucrose solution (pH 7.4). The liposome solutions were frozen and thawed for 3 cycles with liquid nitrogen. Then, the liposome size was adjusted by extruding through polycarbonate filters of 100-nm pore size (Nuclepore, Cambridge, MA). For the preparation of doxorubicin (DOX)-containing liposomes, DOX solutions were added to the initial lipid solutions in the proportion of 30 mol % to the composed lipids (DSPC + DSPG). Unencapsulated DOX was removed by ultracentrifugation at 604,000g for 15 min (HITACHI, Tokyo, Japan), and the amount of DOX in the liposome was determined by measuring the absorbance at 484 nm. The liposome size was measured using ZETASIZER (Malvern Instruments, Malvern, UK).

Cellular uptake of liposomes

The liposomes were radiolabeled by adding [³H]cholesteryl hexadecyl ether solution (370 kBq/mL, GE Healthcare) to the initial lipid solution. HUVECs were seeded (2.0×10^5 cells) on a 35-mm dish and stimulated with rhVEGF as described above. C26 or DU145 cells (both 1.0×10^5 cells) were also

seeded on a 35-mm dish and incubated overnight. The radiolabeled liposomes were added to the cells and further incubated for 2 hr. The cells were washed with PBS and solubilized with 10 mM Tris-HCl buffer containing 0.1% SDS (pH 7.4). The cell lysates were recovered and transferred to HionicFluor (Perkin Elmer, Foster City, CA). Radioactivity was determined with a liquid scintillation counter (LSC-3500; Aloka, Tokyo, Japan).

Intratumoral distribution of WIFPWIQL liposomes

The liposomes were fluorescently labeled by adding the DiI C18 (Molecular Probes, Eugene, OR) solution to the initial lipid solution. C26 cells were subcutaneously implanted into the posterior flank of 5-week-old BALB/c mice. The DiI C18-labeled liposomes were intravenously injected into the mice 10 days after tumor implantation. At 3 or 6 hr after injection of the liposomes, the mice were sacrificed using diethyl ether anesthesia, and the tumors were dissected. Immunostaining was performed as described previously. The tumor tissues were embedded and frozen with dry ice/ethanol. Tumor sections (10 μm) were prepared with cryostatic microtome (HM 505E; Microm, Walldorf, Germany) and air-dried for at least 1 hr. The sections were incubated in 1% bovine serum albumin containing PBS for 10 min at room temperature for protein blocking, with biotinylated anti-mouse CD31 rat monoclonal antibody (BD Pharmingen, Franklin Lakes, NJ) for 18 hr at 4°C, and then with streptavidin-Alexa Fluor 488 conjugates (Molecular Probes) for 30 min at room temperature. Finally, the sections were mounted with Perma Fluor Aqueous Mounting Medium (Thermo Shandon, Pittsburgh, PA) and fluorescently observed with a microscopic LSM system (Carl Zeiss, Germany).

Dorsal air sac model

Dorsal air sac model mice were prepared as follows: C26 cells (1.0×10^7 cells/150 μL) were loaded into a chamber ring (Millipore) covered with filters (0.45-nm pore size, Millipore). The chamber ring was then implanted subcutaneously into the dorsal skin of the mice. At days 2 and 3, 0.3 M sucrose solution (control), PEG-liposomal doxorubicin (PEG-Lip-DOX) or WIFPWIQL-liposomal doxorubicin (WIFPWIQL-Lip-DOX) was intravenously administered (5 mg/kg/day as dose of DOX). At day 4, the mice were sacrificed using diethyl ether and the dorsal skin osculating the chamber ring was observed.

Therapeutic experiment

PEG-Lip-DOX, WIFPWIQL-Lip-DOX (5 mg/kg/day as dose of DOX) or 0.3 M sucrose solution (control) was intravenously administered to the C26-bearing mice at days 6, 9, 12 and 15 after tumor implantation. The tumor size and body weight of each mouse were monitored. The animals used in the experiments were cared for according to the guidelines for the care and use of laboratory animals of the University of Shizuoka.

38